




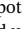












# Multiscale Assessment of Agricultural Consumptive Water Use in California's Central Valley

### Key Points:

- A 30-m daily evapotranspiration product estimated using regionally optimized approach and Landsat Analysis Ready Data Collection 1
- Assessment of agricultural consumptive water use over Central Valley provides critical guidance for sustainable groundwater management
- Large variation of water use was found, mostly due to crop diversity, age structure, and physiological factors

A. J. Wong<sup>1</sup> , Y. Jin<sup>1</sup> , J. Medellín-Azuara<sup>2</sup> , K. T. Paw U<sup>1</sup> , E. R. Kent<sup>1</sup> , J. M. Clay<sup>1</sup> , F. Gao<sup>3</sup> , J. B. Fisher<sup>4</sup> , G. Rivera<sup>4</sup> , C. M. Lee<sup>4</sup> , K. S. Hemes<sup>5</sup> , E. Eichelmann<sup>6</sup> , D. D. Baldocchi<sup>7</sup> , and S. J. Hook<sup>4</sup> 

<sup>1</sup>Department of Land, Air and Water Resources, University of California, Davis, CA, USA, <sup>2</sup>Department of Civil and Environmental Engineering, University of California, Merced, CA, USA, <sup>3</sup>USDA, Agricultural Research Service, Hydrology and Remote Sensing Laboratory, Beltsville, MD, USA, <sup>4</sup>Jet Propulsion Laboratory, California Institute of Technology, Pasadena, CA, USA, <sup>5</sup>Stanford Woods Institute for the Environment, Stanford University, Stanford, CA, USA, <sup>6</sup>School of Biology and Environmental Science, University College Dublin, Dublin, Ireland, <sup>7</sup>Department of Environmental Sciences, Policy, & Management, University of California, Berkeley, CA, USA

### Supporting Information:

Supporting Information may be found in the online version of this article.

### Correspondence to:

A. J. Wong,  
ajywong@ucdavis.edu

### Citation:

Wong, A. J., Jin, Y., Medellín-Azuara, J., Paw U, K. T., Kent, E. R., Clay, J. M., et al. (2021). Multiscale assessment of agricultural consumptive water use in California's Central Valley. *Water Resources Research*, 57, e2020WR028876. <https://doi.org/10.1029/2020WR028876>

Received 18 SEP 2020  
Accepted 28 APR 2021

### Author Contributions:

**Conceptualization:** A. J. Wong, Y. Jin  
**Data curation:** A. J. Wong, J. Medellín-Azuara, K. T. Paw U, E. R. Kent, J. M. Clay, J. B. Fisher, K. S. Hemes, E. Eichelmann, D. D. Baldocchi  
**Formal analysis:** A. J. Wong

**Abstract** Spatial estimates of crop evapotranspiration with high accuracy from the field to watershed scale have become increasingly important for water management, particularly over irrigated agriculture in semiarid regions. Here, we provide a comprehensive assessment on patterns of annual agricultural water use over California's Central Valley, using 30-m daily evapotranspiration estimates based on Landsat satellite data. A semiempirical Priestley-Taylor approach was locally optimized and cross-validated with available field measurements for major crops including alfalfa, almond, citrus, corn, pasture, and rice. The evapotranspiration estimates explained >70% variance in daily measurements from independent sites with an RMSE of 0.88 mm day<sup>-1</sup>. When aggregated over the Valley, we estimated an average evapotranspiration of 820 ± 290 mm yr<sup>-1</sup> in 2014. Agricultural water use varied significantly across and within crop types, with a coefficient of variation ranging from 8% for Rice (1,110 ± 85 mm yr<sup>-1</sup>) to 59% for Pistachio (592 ± 352 mm yr<sup>-1</sup>). Total water uses in 2016 increased by 9.6%, as compared to 2014, mostly because of land-use conversion from fallow/idle land to cropland. Analysis across 134 Groundwater Sustainability Agencies (GSAs) further showed a large variation of agricultural evapotranspiration among and within GSAs, especially for tree crops, e.g., almond evapotranspiration ranging from 339 ± 80 mm yr<sup>-1</sup> in Tracy to 1,240 ± 136 mm yr<sup>-1</sup> in Tri-County Water Authority. Continuous monitoring and assessment of the dynamics and spatial heterogeneity of agricultural evapotranspiration provide data-driven guidance for more effective land use and water planning across scales.

## 1. Introduction

Evapotranspiration, also known as crop consumptive water use in agricultural lands, is often the largest yet most uncertain component of the agricultural water balance in semiarid regions (Burt et al., 2002; Fisher et al., 2017; Oki et al., 2006). Irrigation accounts for 70% of human freshwater use and supports 45% of the world's food supply production (Koech & Langat, 2018). Most irrigation water is lost to the atmosphere via evapotranspiration (California Department of Water Resources, 2020a). Information about evapotranspiration can be applied to optimized sustainable regional water allocations and farm-level irrigation management, improving water, and food security in a changing climate to meet the demands of a growing population (Fisher et al., 2017).

As one of the world's most productive agricultural regions, California is the major producer of various specialty crops including half of the fruits, vegetables, and nuts grown in the United States (California Department of Food and Agriculture, 2018). A quarter of the nation's produce comes from the Central Valley alone, due to its fertile soils and extended growing season, generating \$20 billion of agricultural sales in 2017 (U.S. Department of Agriculture-National Agricultural Statistics Service, 2019). More than 7 million acres (28,000 km<sup>2</sup>) of the Central Valley are irrigated via a system of reservoirs and canals, accounting for about 75% of the state's irrigated lands and consuming about 23 trillion liters of water per year (Faunt, 2009). The acreage of high value yet water-intensive tree crops, such as almonds, pistachios, and walnuts, has been expanding in recent decades, increasing water demand in the state's largest groundwater basin (Strom, 2014).

© 2021 The Authors. This article has been contributed to by US Government employees and their work is in the public domain in the USA. This is an open access article under the terms of the [Creative Commons Attribution-NonCommercial-NoDerivs License](https://creativecommons.org/licenses/by/4.0/), which permits use and distribution in any medium, provided the original work is properly cited, the use is non-commercial and no modifications or adaptations are made.

**Funding acquisition:** Y. Jin, J. Medellín-Azuara, K. T. Paw U, C. M. Lee, D. D. Baldocchi  
**Investigation:** A. J. Wong  
**Methodology:** A. J. Wong, Y. Jin  
**Project Administration:** Y. Jin, J. Medellín-Azuara, K. T. Paw U, C. M. Lee, D. D. Baldocchi, S. J. Hook  
**Software:** A. J. Wong  
**Supervision:** Y. Jin  
**Validation:** A. J. Wong  
**Visualization:** A. J. Wong  
**Writing – original draft:** A. J. Wong  
**Writing – review & editing:** A. J. Wong, Y. Jin, J. Medellín-Azuara, K. T. Paw U, E. R. Kent, J. M. Clay, C. M. Lee, K. S. Hemes, E. Eichelmann, D. D. Baldocchi, S. J. Hook

Groundwater is a major source of water supply in the Central Valley, ranging from 30% during wet years to 70% during extremely dry years (Faunt et al., 2016). During the recent 2012–2016 drought, groundwater pumping was intensified, which led to the doubling of the reduction in the valley's groundwater storage to 11 trillion liters per year from the 2007–2009 value (Xiao et al., 2017). This groundwater overdraft due to excessive pumping accounts for 13% of water sources in the San Joaquin Valley, which is the southern half of the Central Valley (Hanak et al., 2017). It caused significant land subsidence (Faunt et al., 2016), and subsequent damage on aqueducts, costing the state “tens of millions of dollars” in repairs to the aqueduct in the last 40 years (Smith, 2015).

The intensifying drought and reduction in water supply during the summer growing season are expected to continue, due to a projected decrease in snowpack and increasing temperature in the coming decades (Cvijanovic et al., 2017; Lynn, 2015). Consequences of chronic groundwater overdraft and nonpoint sources pollution motivated the enactment of the Sustainable Groundwater Management Act in 2014. It requires local groundwater agencies in critically over-drafted basins to achieve a sustainable water balance by 2040 (California Department of Water Resources, 2019c). Another management challenge under water scarcity is to balance the competing beneficial water uses by many stakeholders, e.g., maintaining river flows to support estuarine habitat (Escriva-Bou et al., 2019). Some potential water management alternatives to attain Sustainable Groundwater Management Act requirements include demand management. For example, via reduced irrigated area, in addition to increasing supply via groundwater recharge. Spatial evapotranspiration estimate records could inform stakeholders on historical and present water demand. Time series of accurate evapotranspiration maps can also help water managers better understand the dynamics of groundwater pumping, improve regulation oversight, and evaluate the impacts of the implemented water policy (Garcia et al., 2016; Hanak, 2011). As 77% of cropland owners in California have fields smaller than 0.4 km<sup>2</sup> (Macaulay & Butsic, 2017), remotely monitoring individual land owner's water use is only possible by using routine satellite observations at a relatively high spatial resolution.

A few algorithms of varying complexity have been developed to map crop evapotranspiration using remote sensing data, due to the large spatial coverage and consistent imagery acquisition by satellite instruments (Akbar et al., 2019; Allen et al., 2007; Anderson et al., 2012; Bastiaanssen et al., 1998; Melton et al., 2012; Nagler et al., 2005; Norman et al., 1995) (Table S1). For example, the crop-coefficient-based evapotranspiration approach has been used by California's growers for irrigation management (California Department of Water Resources, 2005; Melton et al., 2012). This method is relatively easy to implement but does not account for other factors, such as water stress and thus likely overestimates actual evapotranspiration (Anderson et al., 2012; Cuenca et al., 2013). Energy balance-based approaches, on the other hand, estimate evapotranspiration as a residual between available energy and sensible heat flux (Allen et al., 2007; Bastiaanssen et al., 1998; Norman et al., 1995; Su, 2002), for example, as adopted by the Surface Energy Balance Algorithm for Land (SEBAL) (Bastiaanssen et al., 1998) and Mapping EvapoTranspiration at high Resolution with Internalized Calibration (METRIC) (Allen et al., 2007). In METRIC, the sensible heat is often estimated using clusters of hot and cold pixels observed within each Landsat scene (Allen et al., 2007). The pixel selection can be fully automated (Allen et al., 2013) for large-scale applications or manually selected by professional users for more accurate regional estimates.

More sophisticated methods involve solving the soil and canopy latent heat components within a process model, constrained by satellite data (Anderson et al., 2018, 1997; Ryu et al., 2011). The Atmosphere-Land Exchange Inverse (ALEXI) model, for example implements the Two-Source Energy Balance in a time differential mode, based on two snapshots of high temporal frequency geostationary satellite thermal observations, to reduce the sensitivity to the errors in absolute land surface temperatures (Anderson et al., 1997, 2004, 2018). DisALEXI has been further developed to estimate evapotranspiration at 30-m resolution, by bringing in additional higher spatial resolution thermal data from Landsat (Anderson et al., 2012, 2004; Knipper et al., 2018; Norman et al., 2003). A recent comparative study of crop evapotranspiration estimates over the Sacramento-San Joaquin Delta showed that DisALEXI estimates had an RMSE of 1.43 mm day<sup>-1</sup> and mean bias of 0.13 mm day<sup>-1</sup> while the calibrated METRIC prepared by the Irrigation Training & Research Center had an RMSE and mean bias of 2.55 and 2.06 mm day<sup>-1</sup>, respectively (Medellín-Azuara et al., 2018). Another biophysical model, Breathing Earth System Simulator (BESS) (Baldocchi et al., 2019; Jiang & Ryu, 2016; Ryu et al., 2011), couple surface energy balance, photosynthesis, and stomatal conductance processes, to

estimate evapotranspiration, forced by biophysical parameters from Moderate Resolution Imaging Spectroradiometer (MODIS) 8-days 1-km observations.

One compromise between the simple crop-coefficient-based approaches and more complex energy balance models described above is the Priestley-Taylor approach. It estimates evapotranspiration over the wet and extensive surface (De Bruin, 1983; Eichinger et al., 1996; Priestley & Taylor, 1972). It is primarily driven by available energy and a Priestley-Taylor coefficient that partitions available energy to latent and sensible heat. This coefficient was found to be constant for estimating potential evapotranspiration. For drying environmental conditions, Priestley and Taylor (1972) demonstrated that a factor could be added to multiply the Priestley-Taylor evapotranspiration estimates to actual evapotranspiration. They found that the factor remains constant when the cumulative evapotranspiration over a drying surface was below a certain threshold, but the threshold varies from one site to another. After the threshold was exceeded, the scaling factor follows a linear decline to zero after a further 5 cm of evapotranspiration. Similar to Priestley and Taylor (1972)'s concept of scaling Priestley-Taylor evapotranspiration estimates on wet surfaces to actual evapotranspiration over drying surfaces, remote sensing scientists introduced biophysical controls, such as water stress, to down-regulate the Priestley-Taylor coefficient, thus reducing the fraction of available energy used for latent heat. Fisher et al. (2008), for example, parameterized the Priestley-Taylor coefficient separately for soil evaporation, canopy transpiration, and interception using remotely sensed vegetation index and meteorological data. It has been applied to estimate monthly evapotranspiration globally at 5 km and 1° resolutions using Advanced Very High Resolution Radiometer data (Fisher et al., 2008; Vinukollu et al., 2011), regionally at 1 km using MODIS data (Yao et al., 2015) and most recently at 70 m using ECOSystem Spaceborne Thermal Radiometer Experiment on Space Station data (Fisher et al., 2020). Jin et al. (2011) optimized Priestley-Taylor coefficient,  $\alpha$  or  $PT_a$ , as a function of Leaf Area Index (LAI) and soil moisture for each plant function type, using the eddy covariance tower measurements from AmeriFlux sites, and estimated monthly evapotranspiration at 1 km for the entire continental US, from primarily MODIS data.

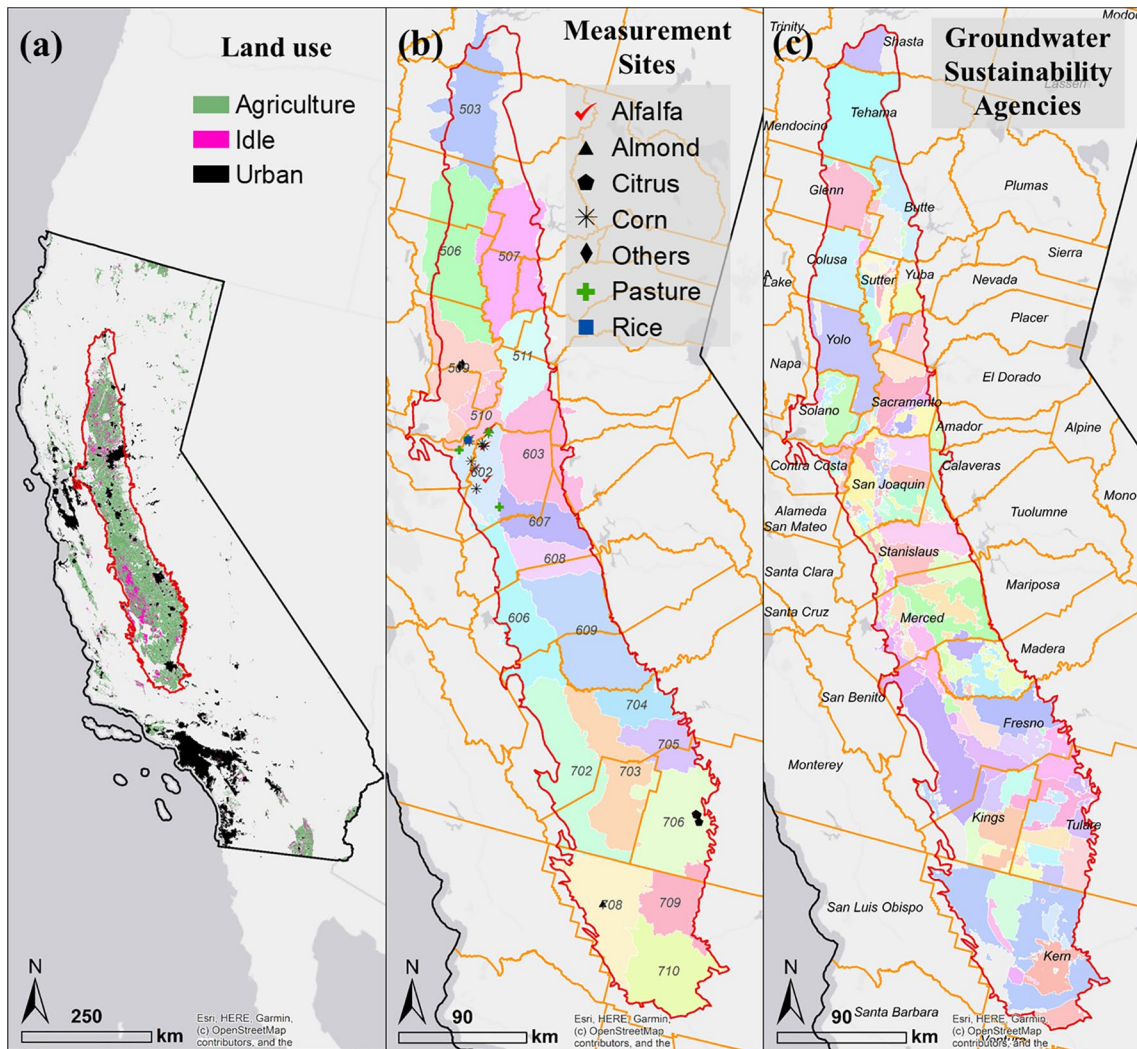
In this study, our primary objective is to improve our understanding of the agricultural water use patterns in California's Central Valley, to facilitate water resources planning, in the context of the Sustainable Groundwater Management Act. We first modified, calibrated, and evaluated the refined semiempirical Priestley-Taylor method (Jin et al., 2011) over major California crops, using the Landsat Analysis Ready Data (Dwyer et al., 2018). This approach further built upon an earlier version adapted for evapotranspiration estimation in Sacramento-San Joaquin Delta (Medellín-Azuara et al., 2018). The method was chosen for this study based on its relatively good performance and computational efficiency for large-scale applications (Medellín-Azuara et al., 2018). The automated workflow for regional applications was applied to assess the spatial patterns of evapotranspiration across the Central Valley and among dominant crop types and to analyze water use changes between 2014 and 2016 water years. To provide insights for water management agencies in their efforts to prepare for droughts and implement Sustainable Groundwater Management Act, we further provided a comprehensive assessment on agricultural evapotranspiration by boundaries of Groundwater Sustainability Agencies (GSAs).

## 2. Data and Methods

We adapted the semiempirical Priestley-Taylor method (Jin et al., 2011), as shown in Equation 1, for agricultural sites in California. The method is driven by Landsat remote sensing data and was calibrated and evaluated using recently available in-situ evapotranspiration measurements, from 2003 to 2019, over a variety of irrigated crop types

$$LE = PT_a * \frac{\Delta}{\Delta + \gamma} * (R_n - G), \quad (1)$$

$\Delta$  represents slope of vapor pressure-temperature curve and  $\gamma$  psychrometric constant. Net radiation ( $R_n$ ) and ground heat flux ( $G$ ) were estimated from Landsat observations.  $PT_a$ , hereafter referred to as the actual Priestley-Taylor coefficient, approximates the fraction of available energy used for actual evapotranspiration. For potential evapotranspiration without any water limitation, the potential Priestley-Taylor coefficient was



**Figure 1.** Study area and locations of measurement sites. Also shown are 2014 agricultural land use (a) over California (black line), County boundaries (orange lines), DWR water planning areas (colored base map) (b), and Groundwater Sustainability Agencies (colored base map) (c) in the Central Valley (red line). DWR, Department of Water Resources.

found to be a constant near 1.26 (Paw U & Gao, 1988). For actual evapotranspiration, we here estimated  $PT_a$  as a function of plant growth and water stress, as shown in Section 2.4.

### 2.1. Study Area

We focused on the major agricultural production area, about 25 thousand km<sup>2</sup>, in the Central Valley of California (Figure 1a). The top eight crop types include almond, grapes, corn, rice, alfalfa, walnuts, pistachios, and tomatoes are based on the updated crop layers from the California Department of Water Resources (DWR) (California Department of Water Resources, 2020b) (Figures 9a, 9c, and 10a). Together, these account for 68% and 73% of agricultural land use in 2014 and 2016, respectively. This semiarid region has a Mediterranean climate, with mild winter and hot, dry summers. Its mean annual precipitation ranges from 51 cm yr<sup>-1</sup> in the north to 13 cm yr<sup>-1</sup> in the far south, and the majority of rainfall occurs from November to March. The Central Valley is therefore highly dependent on irrigation and vulnerable to water scarcity. Its groundwater storage depleted by approximately 16 trillion liters between spring 2005 and 2010 (California Department of Water Resources, 2019a). Groundwater depletion during the recent 2012–2016 drought is expected to be even worse, since Xiao et al. (2017) estimated that the Central Valley's groundwater storage depletion doubled to 11 trillion liters per year from the 2007 to 2009 value.

GSA were established under the Sustainable Groundwater Management Act to manage California's groundwater resources at the local scale. Over 260 GSAs were initially formed in the State's high and medium priority and some are currently under reorganization and consolidation. Figure 1c shows 134 GSAs in the Central Valley that have >1 km<sup>2</sup> of farmland in both 2014 and 2016. The GSAs boundaries are defined by the most recently available DWR's Exclusive GSA map (California Department of Water Resources, 2019b); GSAs boundaries were sometimes split into parts by other political boundaries, so we merged the polygon parts that share an identical GSA name, for example, Byron-Bethany Irrigation District GSA-East Contra Costa and Byron-Bethany Irrigation District GSA—Tracy were merged into a single GSA.

## 2.2. Input Data

### 2.2.1. Field Measurements

A total of 26 evapotranspiration measurement sites over agricultural areas were available in the study region, including five agricultural sites from the AmeriFlux network and two from cropland sites established for the shorter-term study of California's specialty crops (Table 1). The measurement sites represented eight crop types, namely, alfalfa, almond, citrus, corn, pasture, rice, tomato, and beardless winter wheat (Table 1). Evapotranspiration was measured either with an eddy covariance system (Baldocchi et al., 1988; Paw U et al., 2000; Swinbank, 1951) or with a surface renewal system (Paw U et al., 1995). The eddy covariance system uses a sonic anemometer and infrared gas analyzer to measure three-dimensional wind velocities and high-frequency fluctuations of water vapor concentrations (Baldocchi et al., 2001). It measures evapotranspiration by monitoring the vertical flux of water vapor. High-frequency eddy covariance measurements in two alfalfa, two corn, and one rice AmeriFlux sites were collected and preprocessed into half-hourly evapotranspiration data as outlined in Eichelmann et al. (2018) and Hemes et al. (2019). Of the five AmeriFlux sites, net radiation for alfalfa and corn was measured with four-channel net radiometers.

Most sites were located in the Sacramento-San Joaquin Delta region was also employed in the Delta Consumptive Use Comparative Study (Medellin-Azuara et al., 2018) supported by the California State Water Resources Control Board Office of the Delta Watermaster and other agencies. Less expensive surface renewal systems were deployed over 14 sites for corn, alfalfa, and pasture. They use thermocouples to measure sensible heat flux, an NRLITE2 Net Radiometer for net radiation, and either measure ground heat flux ( $G$ ) with a combination of ground heat flux plates and soil thermocouples or assume it is zero for daily estimates. Evapotranspiration is then estimated as the residual of the energy balance. For each crop type, an eddy covariance tower was deployed to calibrate the sensible heat flux relationship between eddy covariance and surface renewal measurements (Castellví et al., 2006; Shapland et al., 2012).

Evapotranspiration measurements were compiled from two specialty crop research projects in Tulare and Kern county of the southern Central Valley, including surface renewal measurements in citrus orchards from 2001 to 2004 (Consoli et al., 2006; Snyder & O'Connell, 2007) and eddy covariance measurements in an almond orchard from 2009 to 2012 (Falk et al., 2013; He et al., 2017). We used only data collected after February 2003 in this study, considering the data availability of California Irrigation Management Information System Spatial product (Spatial-CIMIS) data. The most recently available eddy covariance tower measurements by NASA JPL were also added. The JPL sites were located at the Russell Ranch research field, near Davis, including one over tomato from February to October 2017, and the other over winter wheat from December 2016 to October 2017. These towers have advanced thermal infrared radiometers to measure land surface temperature, and two sets of four channels net radiometers to reduce measurement uncertainty. High-frequency evapotranspiration data were automatically processed using Campbell Scientific Inc.'s standard Eddy-Covariance Datalogger Program software and various quality control procedures. All half-hourly measurements were preprocessed and aggregated into daily evapotranspiration if <20% of the half-hourly measurements were missing within a day.

### 2.2.2. Meteorological Data

We obtained the daily gridded meteorological data, including minimum and maximum-air temperature at 1.5 m, and daily dew point, from Spatial-CIMIS at a 2-km resolution (Hart et al., 2009). The DWR manages a network of over 145 automated weather stations over well-maintained and well-watered grass sites across California providing reference evapotranspiration for pasture. The station data were spatially interpolated

**Table 1**  
*List of In-Situ Measurement Stations and Evapotranspiration Data Availability*

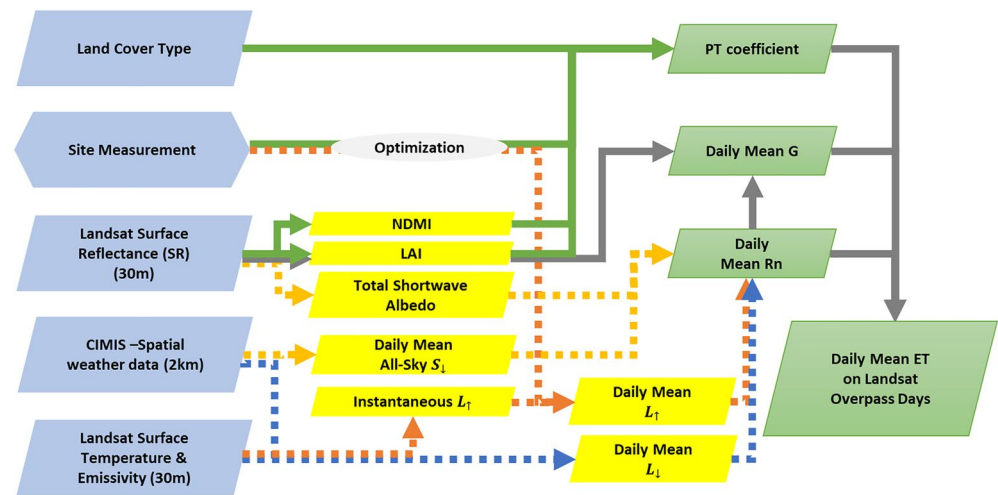
Crop type (site days)	ID	Site	Time period	Citation
Alfalfa (3,870)	1 <sup>a</sup>	US-Tw3: Twitchell Island	May 2013–December 2015	Eichelmann et al., 2018 and Hemes et al., 2018
	2 <sup>a,b</sup>	US-Bi1: Bouldin Island	August 2016–September 2019	Eichelmann et al., 2018 and Hemes et al., 2018
	3 <sup>c</sup>	D02: Staten Island	Mar 2016–April 2017	Medellín-Azuara et al., 2018
	4 <sup>c</sup>	D07: Bouldin Island	July–November 2016	Medellín-Azuara et al., 2018
	5 <sup>c</sup>	D10: Bacon Island	July 2016–April 2017	Medellín-Azuara et al., 2018
	6 <sup>d</sup>	D13: Roberts Island	July 2016–May 2017	Medellín-Azuara et al., 2018
	7 <sup>c</sup>	D14: Twitchell Island	August 2016–December 2016	Medellín-Azuara et al., 2018
Almond (1,405)	8 <sup>a</sup>	A1: Lost Hill	January 2009–December 2011	Couvreur et al., 2016
Citrus (486)	9 <sup>d</sup>	E1: 2-years old	July–August 2004	Consoli et al., 2006
	10 <sup>d</sup>	E2: 4-years old	July–August 2004	Consoli et al., 2006
	11 <sup>d</sup>	E3: 15-years old	July–August 2004	Consoli et al., 2006
	12 <sup>d</sup>	E4: 34+-years old	February 2003–August 2004	Consoli et al., 2006
Corn (1,657)	13 <sup>a</sup>	US-Tw2: Twitchell Island	May 2012–May 2013	Hemes et al., 2018
	14 <sup>a,b</sup>	US-Bi2: Bouldin Island	April 2017–May 2018	Hemes et al., 2018
	15 <sup>c</sup>	D01: Union Island	April 2016–September 2016	Medellín-Azuara et al., 2018
	16 <sup>c</sup>	D06: Holland Island	July–October 2016	Medellín-Azuara et al., 2018
	17 <sup>c</sup>	D08: Bouldin Island	July–September 2016	Medellín-Azuara et al., 2018
	18 <sup>c</sup>	D09: Bacon Island	July–October 2016	Medellín-Azuara et al., 2018
	19 <sup>d</sup>	D11: Staten Island	April–September 2016	Medellín-Azuara et al., 2018
Pasture (697)	20 <sup>c</sup>	D03: Staten Island	May 2016–May 2017	Medellín-Azuara et al., 2018
	21 <sup>c</sup>	D04: Jersey Island	June–November 2016	Medellín-Azuara et al., 2018
	22 <sup>c</sup>	D05: Ripon Island	June 2016–January 2017	Medellín-Azuara et al., 2018
	23 <sup>d</sup>	D12: Twitchell Island	June 2016–December 2016	Medellín-Azuara et al., 2018
Rice (2,909)	24 <sup>a</sup>	US-Twt: Twitchell Island	April 2009–April 2017	Baldocchi et al., 2016
Tomato (112)	25 <sup>a,b</sup>	RR2: Russell Ranch	January 2017–November 2017	Cawse-Nicholson et al., 2017
Winter wheat (102)	26 <sup>a,b</sup>	RR1: Russell Ranch	January 2017–October 2017	Cawse-Nicholson et al., 2017

<sup>a</sup>Eddy covariance. <sup>b</sup>Reserved for independent validation. <sup>c</sup>Lite surface renewal system estimates daily evapotranspiration by assuming the daily mean  $G$  is zero. <sup>d</sup>Full surface renewal system.

to produce the 2-km gridded data set since 2003. We also used the Spatial-CIMIS cloud cover and incoming solar radiation for both clear-sky and all-sky conditions, derived from Geostationary Operational Environmental Satellite visible channel imager data, for our radiation component calculation.

### 2.2.3. Remote Sensing Data

All available surface reflectance and surface temperature products, and the corresponding quality assessment layers at 30 m were downloaded from USGS Landsat Analysis Ready Data set (Dwyer et al., 2018). A total of eight tiles covered the whole study area. The land surface temperature retrieval from the Landsat thermal data is based on a radiative transfer model with an improved surface emissivity estimate (Cook, 2014). Each active Landsat satellite takes snapshots between 9:53 and 10:55 a.m. Pacific Standard Time every 16 days. Invalid or high uncertainty pixel values were filtered based on the quality assessment rasters, including SLC gaps (U.S. Geological Survey, 2016), snow, cloud/cloud shadow, for example, a high value for cloud or cirrus confidence, or with a surface temperature uncertainty greater or equal to 6 K. For model calibration and validation purposes, a single pixel near each measurement site was extracted.



**Figure 2.** The flowchart of estimating daily evapotranspiration at 30 m during clear-sky Landsat overpassing day.

### 2.3. Estimating Daily Net Radiation and Ground Heat Flux From Landsat Observations

We estimated surface net radiation ( $R_n$ ) at a daily time scale as shown in Equation 2

$$R_n = (1 - \text{Albedo}) * S_{\downarrow} + \left[ \varepsilon_s \varepsilon \sigma T_a^4 - \left( m * (\varepsilon_s \sigma T_s^4) + b \right) \right], \quad (2)$$

where  $S_{\downarrow}$  and  $T_a$  are daily mean all-sky incoming solar radiation and daily mean air temperature ( $T_a$ ), from CIMIS-Spatial (Hart et al., 2009),  $\varepsilon$  represents all-sky emissivity for the atmosphere,  $\varepsilon_s$  surface emissivity,  $T_s$  for instantaneous land surface temperature in Kelvin from Landsat surface temperature product (Figure 2). Two parameters ( $m$  and  $b$ ) to be optimized were included here to convert the estimated instantaneous outgoing longwave radiation ( $L_t$ ) to daily mean values. Shortwave surface albedo was derived at 30 m from the Landsat surface reflectance using the narrowband to broadband conversion coefficients (Liang, 2001).

To calculate the incoming longwave radiation ( $L_{\downarrow}$ ), the approach of Jin et al. (2011) was followed to estimate all-sky emissivity ( $\varepsilon$ ) as a function of cloud fraction ( $F$ ) and clear-sky emissivity ( $\varepsilon_{\text{clr}}$ ),  $\varepsilon = (1 + \mu * F^V) * \varepsilon_{\text{clr}}$ . Cloud fraction is computed by subtracting 1 by the ratio of Spatial-CIMIS's all-sky and clear-sky incoming solar radiation. In this study, the parameters  $\mu = 0.242$  and  $V = 0.583$  (Duarte et al., 2006) were used.  $\varepsilon_{\text{clr}}$  was estimated with CIMIS-Spatial's dew point temperature.

We developed a different approach from Jin et al. (2011) to estimate the daily mean outgoing longwave radiation ( $L_t$ ) from the land surface, considering there is only one Landsat overpassing time around 10:30 a.m. as compared to four from MODIS Terra and Aqua. The instantaneous outgoing longwave radiation was first estimated with Landsat land surface temperature and surface emissivity product (Cook, 2014), and then transformed to daily mean values through a linear relationship, as shown by two parameters ( $m$  and  $b$ ) in Equation 2. We optimized this linear function, with the field measurements of half-hourly longwave radiation, only available from sites 1 and 13 from the training data set during clear-sky overpassing days. A piecewise linear regression was used from the Shape Language Modeling toolbox (D'Errico, 2020), based on the site measurements of half-hourly longwave radiation, available from sites 1 to 13 from the training data set during clear-sky overpassing days.

Ground heat flux ( $G$ ) was estimated from an empirical relationship of  $R_n$  and fractions of vegetation and soil ( $f_{\text{veg}}$ ,  $f_{\text{soil}}$ ) as described in Jin et al. (2011), where  $f_{\text{soil}} = e^{-0.4 \text{LAI}}$ ,  $f_{\text{veg}} = 1 - f_{\text{soil}}$ , and  $G = -4.6144 + (0.0496 f_{\text{veg}} + 0.1048 f_{\text{soil}}) R_n$ . We adopted PT-JPL's approach in estimating LAI using normalized difference vegetation index (NDVI), where  $\text{LAI} = -\log(1 - (\text{NDVI} - 0.05)) / 0.3$  (Fisher et al., 2008). NDVI, calculated based on the Landsat reflectance at red and near-infrared, has been widely used as an indicator of green vegetation cover and biomass (Tucker, 1979).

#### 2.4. Actual Priestley-Taylor Coefficient Optimization

The actual Priestley-Taylor coefficient  $PT_a$  in Equation 1 was parameterized as an empirical function of LAI, moisture condition, and air temperature, as shown in

$$PT_a = (A - C * e^{-B*LAI}) * (D * (NDMI + 1) + E) * f(T_a), \quad (3)$$

where  $A$ ,  $B$ ,  $C$ ,  $D$ , and  $E$  are parameters to be optimized, and  $f(T_a)$  was a relatively weak temperature control, due to the warm weather in the valley, that is, lowered to 0.05 only if  $T_a$  is lower than  $-5$  C, otherwise having the value of 1 (Jin et al., 2011). The soil-moisture constraint was replaced with a remote sensing-based normalized difference moisture index (NDMI) (Gao, 1996; Ji et al., 2011), due to the lack of volumetric soil moisture data and the practical consideration in implementing a water balance model as used in Jin et al. (2011) study. NDMI is calculated from Landsat reflectance at two bands, the near-infrared centered at  $0.86 \mu\text{m}$  and the shortwave infrared band centered at  $1.61 \mu\text{m}$ . It has been used as an indicator of plant water conditions due to strong absorption by liquid water in the shortwave infrared region (Gao, 1996; Ji et al., 2011).

The five parameters ( $A$ ,  $B$ ,  $C$ ,  $D$ , and  $E$ ) in Equation 3 were optimized with daily data from field observations. For each crop type that had field measurements, we used the nonlinear least-squares optimization procedure in MatLab Optimization Toolbox (MATLAB, 2018), to minimize the difference between the predicted actual Priestley-Taylor coefficients and those derived from the daily means of field measurements. We randomly split the measurement data during all days when Landsat overpassing days were not obscured by cloud, into training (70%) and testing subsets (30%) for each site. To test the robustness of the algorithm, we repeated this random selection procedure 1,000 times. For crop types that had seven stations, that is, alfalfa and corn, modified k-fold cross-validation was further performed, with a “leave-two-out” approach, where all data from two stations were reserved for independent testing at a time, while the rest used for calibration.

To estimate evapotranspiration for crop types where field measurements were not available, a generalized optimization was also developed, where the data were pooled from all crops together for one universal set of optimization. This was done by randomly selecting a maximum of 50 points for each crop from the training data set mentioned above, due to the unevenly available sample size among crop types. Similar to the crop-specific optimization, we also conducted two types of cross-validations to test the robustness of the generalized method.

#### 2.5. Daily Evapotranspiration Estimation

During cloud-free days with Landsat overpasses, Landsat-derived LAI and NDMI were fed into Equation 3 to estimate the actual Priestley-Taylor coefficient for each pixel, which was then combined with available energy ( $R_n - G$ ) to estimate daily evapotranspiration (Figure 2). For days between Landsat overpasses (or pixels) without valid or high-quality values such as cloudy days or over scan-line corrector data gaps (Storey et al., 2005), a temporal interpolation approach was adopted (Allen et al., 2007; He et al., 2017). First, daily evapotranspiration estimates, during the adjacent clear-sky Landsat days and within  $\pm 2$  months search window, were divided by the concurrent Spatial-CIMIS daily reference evapotranspiration to derive the fraction of reference evapotranspiration (EToF). A shape-preserving piecewise cubic interpolation was applied to this discrete time series of EToF to obtain a continuous time series of daily EToF. We set a requirement of a minimum of 2 valid observations within the search window for a robust interpolation. This temporal interpolation was needed mostly during rainy season in winter and early spring in California, an off-season for the majority of the crops. Finally, daily evapotranspiration for missing days was estimated as a product of the interpolated EToF and Spatial-CIMIS reference evapotranspiration.



## 2.6. Validation and Uncertainty Analysis

The uncertainty of  $R_n$ , actual Priestley-Taylor coefficient, and daily evapotranspiration, directly estimated by our approach during clear-sky Landsat overpass days, was evaluated by comparison with the field measurements in the training, testing, and the full data sets, respectively. Four metrics were used to evaluate the method performance, including  $R^2$ ,  $1 - \left( \frac{\sum_{i=1}^n (P_i - M_i)^2}{\sum_{i=1}^n (M_i - \bar{M})^2} \right)$ , also known as Nash-Sutcliffe model efficiency coefficient; root mean squared error (RMSE), bias, where  $\text{Bias} = \sum_{i=1}^n (P_i - M_i) / n$ , and relative mean absolute difference (RMAD),  $\text{RMAD}(\%) = \frac{\sum_{i=1}^n (|P_i - M_i|)}{\sum_{i=1}^n (M_i)} * 100\%$ , where  $P$  and  $M$  are remote sensing estimates and field measurements, respectively. We also summarized the statistics of the results from the cross-validations, including the variance of the optimized parameters in Equation 3, and the corresponding estimates of Priestley-Taylor coefficient and evapotranspiration values.

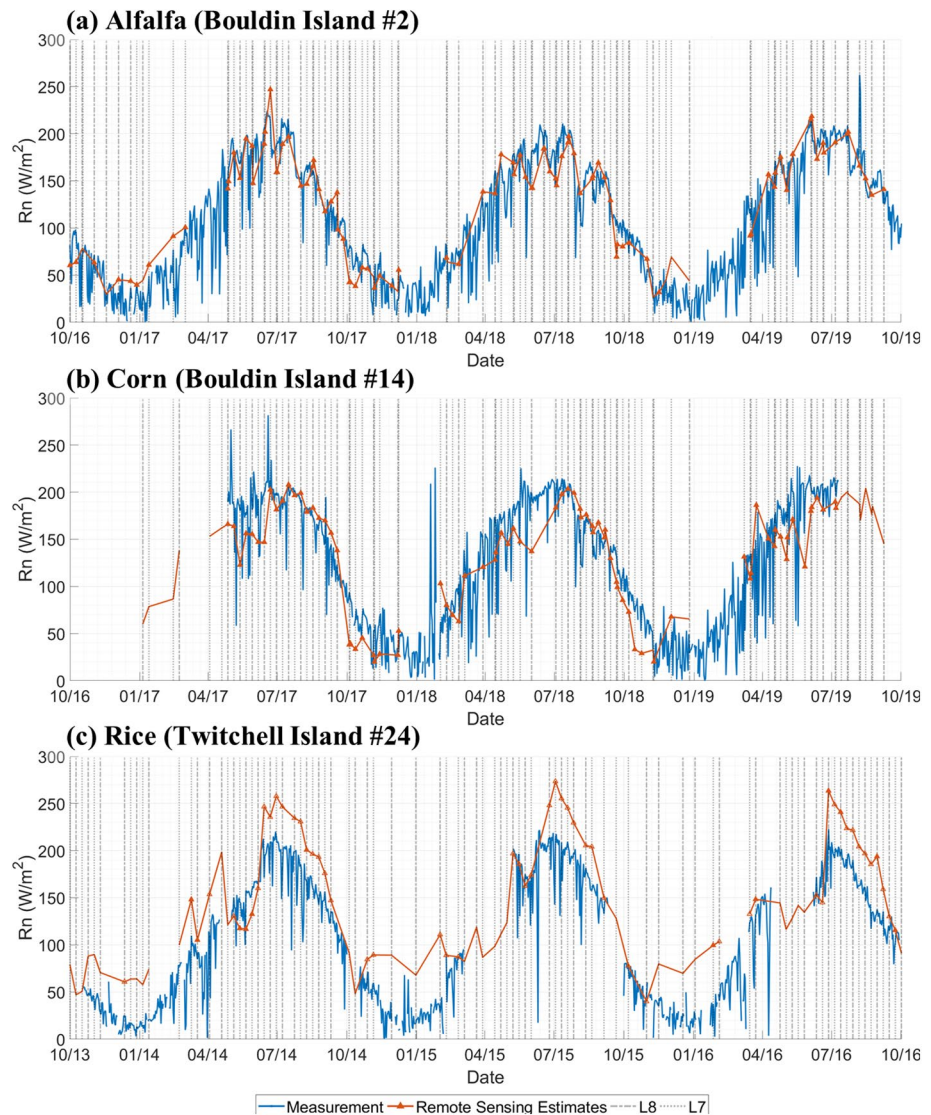
Values of daily evapotranspiration that involved temporal interpolation were further evaluated during non-Landsat overpassing or cloudy days. An evaluation was also done for continuous daily, weekly, and monthly evapotranspiration estimates. The uncertainty introduced by the generalized optimization was also analyzed.

To compare our refined approach, hereafter referred to as PT-UCD, with previous Priestley-Taylor approaches, we calculated the actual Priestley-Taylor coefficients and evapotranspiration for all sites during clear-sky Landsat overpass days, following Jin et al. (2011)'s and Fisher et al. (2008)'s methods, hereafter referred to as PT-0 and PT-JPL, respectively. All methods were driven by the same forcing data here, for example,  $R_n$ , CIMIS-Spatial meteorological data, to evaluate the difference caused by the methods themselves. PT-0 did not apply the soil-moisture constraint for irrigated crops, and therefore its actual Priestley-Taylor coefficients equation can be simplified as  $\alpha = 1.22 \left( 1 - e^{-3.48 LAI} \right) * f(T_a)$ . To estimate PT-JPL evapotranspiration using Landsat time series data, we modified PT-JPL's publicly accessible code (Fisher, 2008), which was written to estimate spatial evapotranspiration using monthly Advanced Very High Resolution Radiometer and The International Satellite Land Surface Climatology Project, Initiative II data (see Text S1 for details).

## 2.7. Regional Evapotranspiration Patterns

The Priestley-Taylor method optimized here was applied over the whole California Central Valley to estimate crop evapotranspiration during the 2014 and 2016 water years. The crop-specific actual Priestley-Taylor coefficient parameterization results were used for daily averaged evapotranspiration estimation over alfalfa, almond, corn, citrus, pasture, and rice areas during Landsat overpassing days. For remaining crop types, including but not limited to grapes, walnut, pistachio, tomatoes, wheat, and cotton, where no field evapotranspiration data were available for crop-specific optimization, the generalized actual Priestley-Taylor coefficient parameterizations was applied. Temporal interpolation was applied to derive a complete time series of daily evapotranspiration for each Landsat pixel. For each month, an EToF pixel is interpolated only if there are at least two estimates on clear-sky overpassing days with a  $\pm 2$  months moving time window; the uninterpolated pixels were gap-filled by multiplying daily reference evapotranspiration by EToF averaged by corresponding month and crop within each Landsat Analysis Ready Data tile. Daily evapotranspiration estimates were further averaged to annual time scales to analyze the regional patterns. Evapotranspiration was summarized for each crop type and compared the differences among crops by evaluating the annual evapotranspiration, reference evapotranspiration, and EToF. Specifically, the per-area water consumptive use average was computed by dividing the sum of annual evapotranspiration by crop area over nongap-filled pixels, while total consumptive use was computed over all crop area pixels.

We further summarized annual evapotranspiration by GSA boundaries to provide agricultural water use information for water planning. This was achieved by quantifying annual water use and variability for each planning area and compared across areas. We also analyzed the association of water use with corresponding land use,  $R_n$ , actual Priestley-Taylor coefficient, EToF, and reference evapotranspiration, to understand what contributed to water use differences among GSAs. While GSAs manage local groundwater resources, DWR oversees water resources regionally by water planning area. We summarized our annual crop evap-



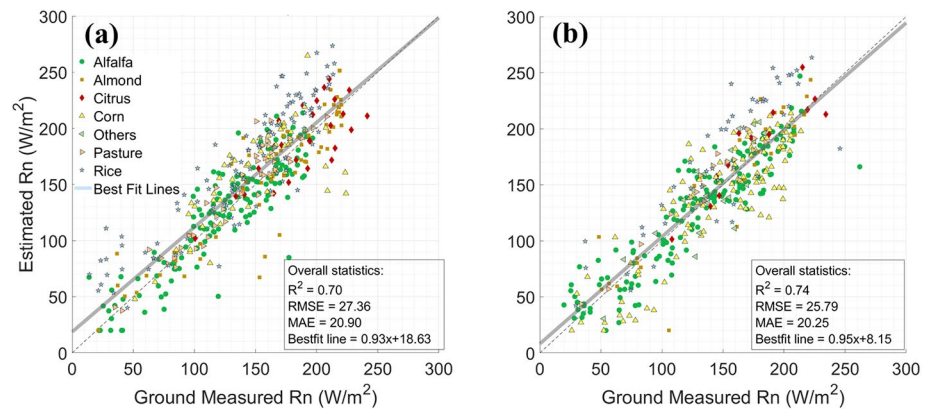
**Figure 3.** Time series of  $R_n$  from daily measurements (blue) and estimates on clear-sky overpassing days (red) over (a) an alfalfa site at Bouldin island (#2); (b) a corn site at Bouldin island (#14); and (c) a rice site at Twitchell Island (#24). The overpassing days of Landsat 7 and 8 are indicated by the vertical dash lines in gray.

otranspiration estimates by water planning areas in the Central Valley and compared them with DWR's estimates for the water year 2014.

### 3. Results

#### 3.1. Net Radiation and Available Energy

The  $R_n$  estimated from our approach captured similar seasonal dynamics as observed by field measurements (Figure 3). For example, estimated  $R_n$  was close to  $20 \text{ W m}^{-2}$  in January, increased continuously to  $200 \text{ W m}^{-2}$  in June over an example alfalfa site (#2) and corn site (#14), and then started to decrease in July, reaching around  $75 \text{ W m}^{-2}$  in October. An overestimation of  $R_n$  was found over Rice, mostly when the fields were flooded, e.g., during the growing season from April to October (Knox et al., 2016) and in winter. There is also a recurring underestimation of corn's  $R_n$  in between April and July for both sites 13 and 14, but not sites 15 and 19.



**Figure 4.** Comparison of remote sensing-derived  $R_n$  vs. field measurements over all sites, from (a) training data ( $N = 447$ ) and (b) testing data set ( $N = 389$ ).

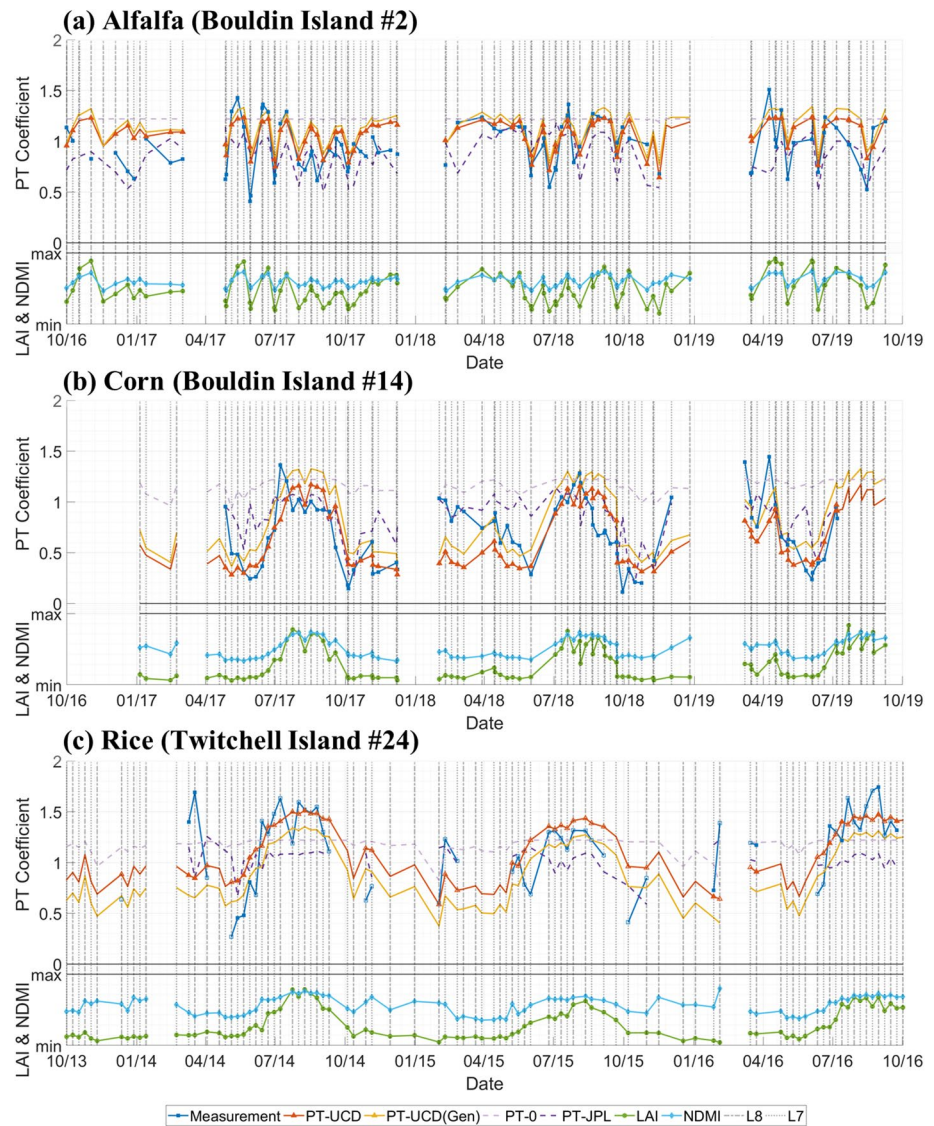
Overall the remote sensing-derived  $R_n$  agreed well with  $R_n$  measurements across all sites and overpassing days, with an overall  $R^2$  of 0.74, an RMSE of  $25.8 \text{ W m}^{-2}$ , and an RMAD of 14.3% for the testing subset (Figure 4b). Only a small bias of  $1.70 \text{ W m}^{-2}$  was found. The agreement was similar to the training subset, with an  $R^2$  of 0.70 and an RMSE of  $27.4 \text{ W m}^{-2}$  (Figure 4a). The uncertainties of  $R_n$  estimate varied by crop type, with the highest accuracy found for alfalfa, citrus, and pasture while relatively larger uncertainty for rice. Note that both evaluations using training and testing data sets were informative about the model's uncertainty because there was only one calibration for our  $R_n$  estimate, converting the instantaneous to daily outgoing longwave radiation on clear-sky Landsat overpassing days, which used only two sites ( $n = 94$ ) in the training data set.

### 3.2. Actual Priestley-Taylor Coefficients

The seasonal dynamics of the actual Priestley-Taylor coefficient typically followed the plant growth curve, as shown by the values derived from both the field measurements and satellite observations (Figure 5). For example, the actual Priestley-Taylor coefficients of alfalfa frequently fluctuated from 0.5 to 1.5, likely due to the multiple cuttings throughout the growing season, as shown by the similar variations in LAI (Figure 5a). Field measurements showed a substantial seasonal variation in the actual Priestley-Taylor coefficient for the corn and rice sites, e.g., with towering peaks in summer growing season, a relatively small peak in spring, and much lower values in between fall and winter (Figures 5b and 5c).

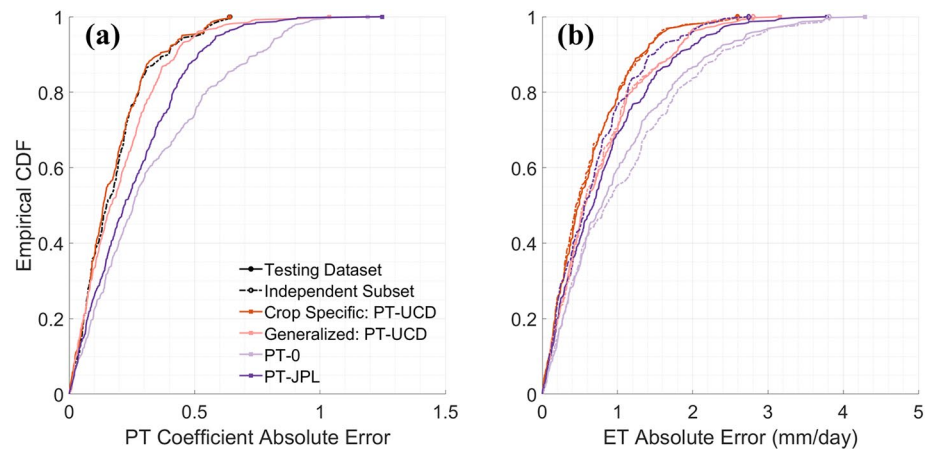
In general, the remote sensing-derived actual Priestley-Taylor coefficients, from the crop-specific optimization, could explain 56% of the variance observed across sites and time periods, with an RMSE and RMAD of 0.23% and 17.7%, when compared with the field-based estimates over the testing data set (Figure S1). For the generalized optimization, the uncertainties of actual Priestley-Taylor coefficient estimates increased slightly (e.g.,  $R^2 = 0.50$ , RMSE = 0.26, and RMAD = 21.64%). Among crop types, both crop-specific and generalized actual Priestley-Taylor coefficient estimation performs best for almond (RMAD = 8.2% and 9.4%). The performance of the crop-specific actual Priestley-Taylor coefficient is significantly better than the generalized actual Priestley-Taylor coefficients for corn and citrus.

The actual Priestley-Taylor coefficient estimates showed significant improvement when compared to those derived from PT-0, which only captured small seasonal variation (25%) and had a higher bias of 0.24 and a larger RMAD of 34.7% over the irrigated cropland in the valley (Figure 5). In contrast, PT-JPL estimates showed a reasonable seasonal pattern for alfalfa and corn (Figures 5a and 5b), although it was not calibrated for any land cover type (RMSE = 0.32 and RMAD = 27.3%). Across all sites, the crop-specific PT-UCD showed an overall improvement over PT-JPL, as shown by the empirical cumulative distribution function of the absolute errors when compared to both testing and independent testing data (Figure 6a). For example, 88% of testing samples had an absolute error were below 0.30 from crop-specific PT-UCD estimates, compared to 62% and 59% from PT-JPL and PT-0 estimates, respectively. The generalized PT-UCD performed only slightly better than PT-JPL (Figure 6a).



**Figure 5.** Time series of crop-specific (red) and generalized (yellow) PT coefficients derived from tower observations and remote sensing, over the same three sites as shown in Figure 3. The unfilled symbols on overpassing dates indicate that the data point was previously partitioned into the training data set. The estimates from the other two PT approaches, namely PT-0 and PT-JPL, were also shown for comparison. The lower panel shows the corresponding LAI and NDMI in green and cyan, ranging from 0 to 7 and  $-1$  to 1, respectively. All three Priestley-Taylor methods shown here were driven with the same forcing data.

Two types of cross-validation testing further showed the optimization of the parameters in Equation 3 for estimating the actual Priestley-Taylor coefficient was reasonably robust. The distribution of the estimated parameters showed a very small variance, for the majority of the crops and the generalized optimization (Table S2). One exception was parameter  $D$ , which represented the moisture regulation over the coefficient, for citrus and pasture (typically well-watered). The estimated actual Priestley-Taylor coefficients were shown to be stable among the repeat and leave-two-out cross-validations (Figures S2–S5), with an Inter Quantile Range (IQR) of RMAD of  $<5\%$  (Figure S2).



**Figure 6.** Comparison of empirical cumulative distribution errors among estimated (a) PT coefficient and (b) evapotranspiration using four models on clear-sky Landsat overpassing days. All three Priestley-Taylor methods shown here were driven with the same forcing data.

### 3.3. Evapotranspiration Estimates

#### 3.3.1. Daily Mean Evapotranspiration on Clear-Sky Landsat Overpassing Days

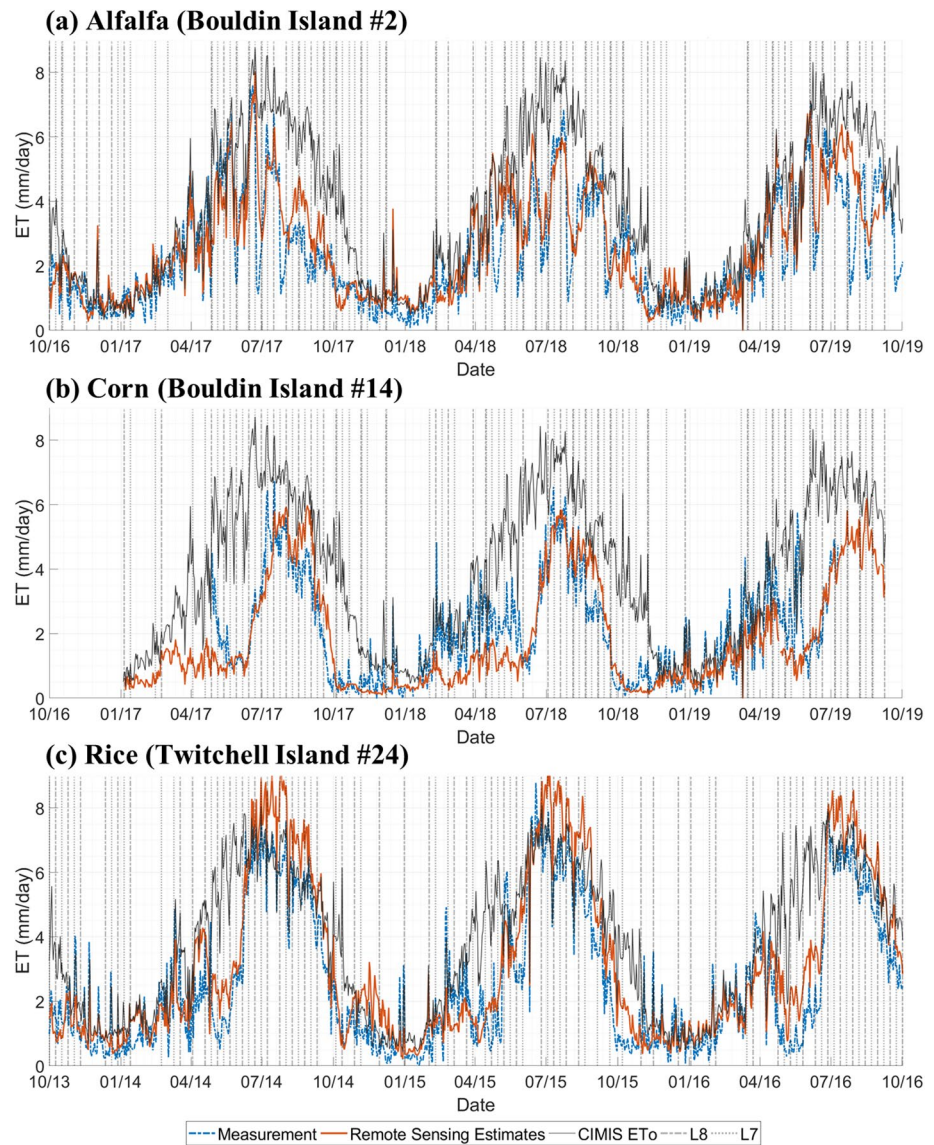
We found a good agreement between field measurements of evapotranspiration and satellite-based estimates during the clear-sky days with Landsat acquisitions. When evaluated with the testing data set, both the crop-specific and generalized evapotranspiration models captured the seasonal variability well (Figure 7). Across all sites, the crop-specific evapotranspiration had an  $R^2$  of 0.79, RMSE of  $0.90 \text{ mm day}^{-1}$ , and RMAD of 20.5% (Figure 8b). Only a small bias of  $0.14 \text{ mm day}^{-1}$  was found. When using the generalized actual Priestley-Taylor coefficients, slightly higher uncertainties were found, with an  $R^2$  of 0.76, RMSE of  $0.98 \text{ mm day}^{-1}$ , and RMAD of 23.1% (Figure 8d).

The performance of evapotranspiration estimates varied by crop types. When using the crop-specific Priestley-Taylor optimization, the RMSE and RMAD ranged from  $0.68$  to  $1.34 \text{ mm day}^{-1}$  and 13.3% to 28.4%, based on the comparison with the testing data set (Table 2). The best performance was found for alfalfa, citrus, and pasture sites, while the weakest performance in rice. The generalized approach also performed the best for alfalfa and citrus and performed the poorest for rice and corn (Figures 8, S3, and Table S4). The leave-two-out cross-validation showed relatively small differences in RMSEs of daily ET estimates from site to site (Figure S4), e.g.,  $0.7 \text{ mm day}^{-1}$  in alfalfa site #6 vs.  $0.9 \text{ mm day}^{-1}$  in site 5 based on the results from alfalfa-specific optimization, and  $0.7$ – $1.2 \text{ mm day}^{-1}$  among the corn sites.

Crop-specific PT-UCD showed an improvement over PT-0, PT-JPL, and generalized PT-UCD. About 80% of crop-specific evapotranspiration estimates in the testing and independent data set had an error of  $<1 \text{ mm day}^{-1}$ , as shown by the empirical cumulative distribution functions of the absolute errors between the daily crop-specific evapotranspiration estimates and field measurements (Figure 6b). In contrast, both generalized PT-UCD and PT-JPL appeared to perform similarly, that is, about 70%–76% of samples had an evapotranspiration error  $<1 \text{ mm day}^{-1}$ , and about 85%–90%  $<1.5 \text{ mm day}^{-1}$ . However, for the PT-0 evapotranspiration estimates, only 55% and 70% of samples had an error  $<1$  and  $1.5 \text{ mm day}^{-1}$ , respectively.

#### 3.3.2. Continuous Evapotranspiration Estimates

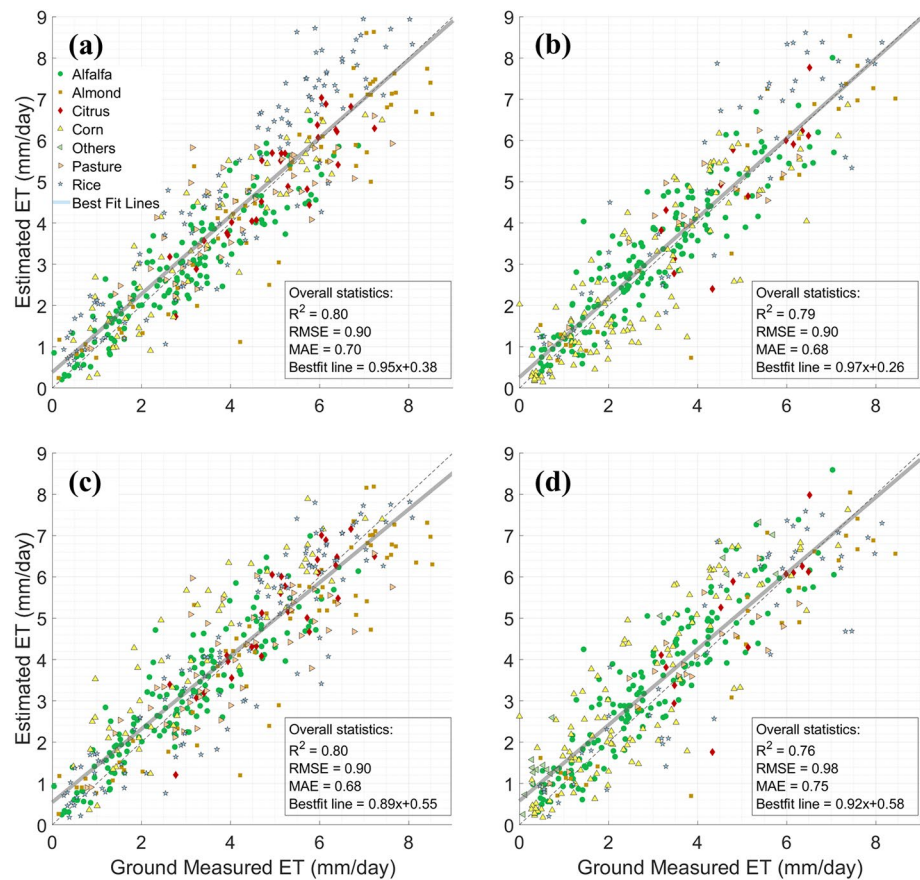
The interpolation of EToF from adjacent overpassing days introduced a small overall uncertainty in daily evapotranspiration estimates, for example, RMSE increased by  $0.10$ – $0.17 \text{ mm day}^{-1}$  and decreased  $R^2$  by  $0$ – $0.08$  when estimating evapotranspiration for alfalfa, citrus, corn, and pasture (Tables 2 and S6). When further aggregated to weekly and monthly time scales, the satellite-derived evapotranspiration estimates agreed better with those from the field measurements (Figures S8c and S8d). For example, across all sites,  $R^2$  was increased to 0.83 and 0.88, and RMSE reduced to  $0.79$  and  $0.65 \text{ mm day}^{-1}$ , respectively, for weekly and monthly evapotranspiration values based on the crop-specific Priestley-Taylor optimization.



**Figure 7.** Time series of crop-specific and interpolated daily evapotranspiration estimates vs. measurement.

### 3.4. Evapotranspiration Patterns and Dynamics Over the Central Valley

We estimated a total of 19.9 and 21.8 tera-liter of water consumption via evapotranspiration over the agricultural land in California's Central Valley in 2014 (24.1 thousand km<sup>2</sup>) and 2016 water years (25.8 thousand km<sup>2</sup>), respectively (Figures 9c and 9d). In the water year 2014, the top eight crop types accounted for 75% of total crop consumptive water use in the valley, including almond (22.2%), rice (10.2%), grapes (9.4%), alfalfa (9.4%), corn (8.9%), walnuts (7.3%), pistachios (4.1%), and tomatoes (3.6%) (Figures 10a and 10b). Overall, rice was the second largest water consumer after almonds, although it only used 7.6% of cropland, due to its highest annual evapotranspiration rate of 1,109 ( $\pm 85$ ) mm yr<sup>-1</sup>, on a per unit area basis (Figure 10c). Pasture, walnut, almonds, citrus, and alfalfa also had relatively high evapotranspiration rate (greater than 800 mm yr<sup>-1</sup>) (Figure 10c) (Table S7). In contrast, wheat consumed the least amount of water per area (561  $\pm$  228 mm yr<sup>-1</sup>) among major crops, whereas pistachio, tomato, corn, cotton, and grapes had a moderate evapotranspiration rate between 600 and 800 mm yr<sup>-1</sup>. As the second and third largest cropland use in the valley, grapes, and corn used less total water than rice but similar water with alfalfa, walnuts, and fruits.



**Figure 8.** Comparison of remote sensing-derived daily evapotranspiration vs. field measurements on Landsat overpassing days over all sites, based on (a) training data ( $N = 345$ ) and (b) testing data set ( $N = 149$ ), when using crop-specific optimization parameters. The corresponding results from the generalized optimization are shown in (c) and (d).

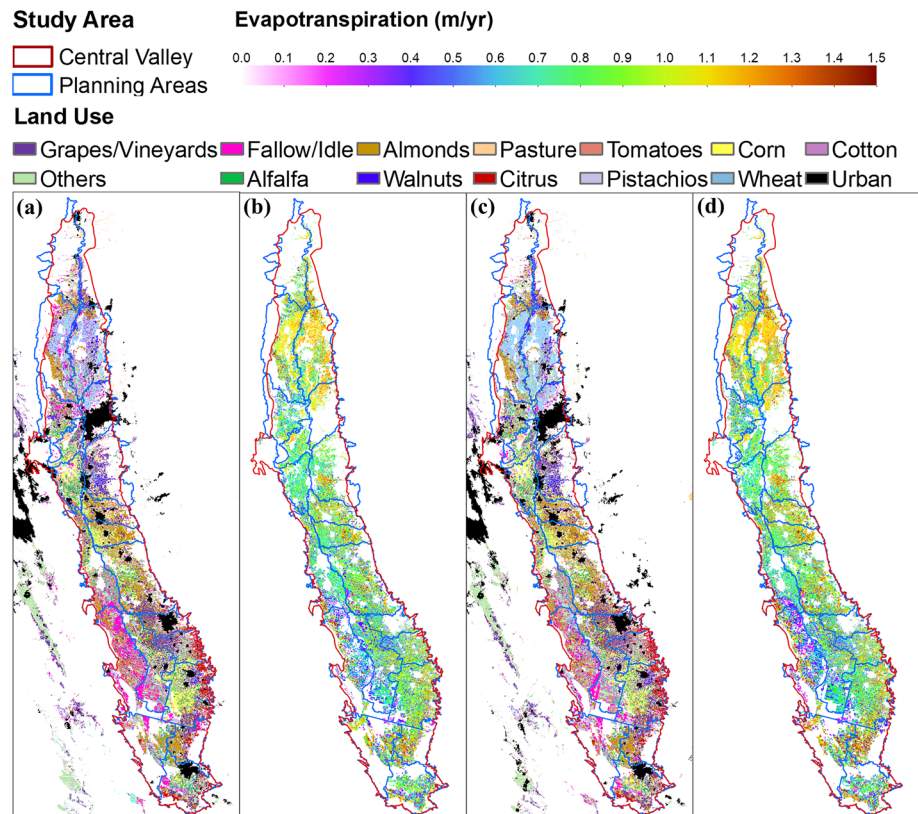
Across the valley, the mean annual evapotranspiration rate varied by 35% ( $820 \pm 290 \text{ mm yr}^{-1}$ ) over all agricultural pixels in 2014, mostly due to the diversity of the crop types. We also found high variability of evapotranspiration rate within each crop type, especially over orchards such as almond, pistachios, and

**Table 2**

Comparison of Daily Evapotranspiration Estimates From Three Priestley-Taylor Approaches With Field Measurements During Days With Clear-Sky Landsat Observations and Other Days (From Temporal Interpolation)

Crop types	$R^2$				RMSE ( $\text{mm day}^{-1}$ )			
	PT-0		PT-JPL		PT-UCD		PT-UCD	
	Clear-sky overpassing days		Interpolated		Clear-sky overpassing days		Interpolated	
Alfalfa	0.64 (0.57)	0.69 (0.71)	0.83 (0.82)	0.75	0.94 (1.05)	0.87 (0.86)	0.65 (0.68)	0.77
Almond	0.78 (0.78)	0.48 (0.53)	0.85 (0.86)	0.89	1.13 (1.18)	1.73 (1.72)	0.95 (0.94)	0.86
Citrus	0.40 (0.24)	<0 (<0)	0.70 (0.56)	0.70	0.99 (1.08)	1.39 (1.48)	0.69 (0.83)	0.86
Corn	0.18 (0.11)	0.72 (0.70)	0.75 (0.71)	0.68	1.65 (1.66)	0.97 (0.97)	0.91 (0.96)	1.01
Pasture	0.75 (0.66)	0.42 (0.36)	0.77 (0.72)	0.69	0.86 (0.86)	1.31 (1.81)	0.82 (0.77)	0.94
Rice	0.80 (0.77)	0.80 (0.72)	0.75 (0.67)	0.77	1.03 (1.11)	1.03 (1.25)	1.16 (1.34)	1.09
All (crop-specific)	N/A	N/A	0.81 (0.79)	0.80	N/A	N/A	0.87 (0.90)	0.93
All (generalized)	0.70 (0.57)	0.70 (0.71)	0.80 (0.76)	0.78	1.15 (1.32)	1.12 (1.07)	0.91 (0.98)	0.95

Note. For clear-sky overpassing days, statistics were based on the full data set, the testing data set only (in parenthesis), respectively.



**Figure 9.** Spatial distributions of (a, c) land use and (b, d) annual evapotranspiration ( $\text{m yr}^{-1}$ ) over the Central Valley in 2014 and 2016 water years, respectively.

walnut, with a CV higher than 20% (Table S7), most likely due to differences in planting density, age, canopy structures, and stressors among orchards (Ferguson et al., 2005). For example, the almond evapotranspiration rate varied by 34% ( $964 \pm 328 \text{ mm yr}^{-1}$ ), and the rate for pistachio varied by 59% ( $592 \pm 352 \text{ mm yr}^{-1}$ ) in 2014. Wheat also had a very high variability (CV: 41%), different from other annual crops, which typically had a much lower variation of evapotranspiration rate than perennial crops. For all major crop categories, the difference in CV between 2014 and 2016 was  $<7.2\%$ .

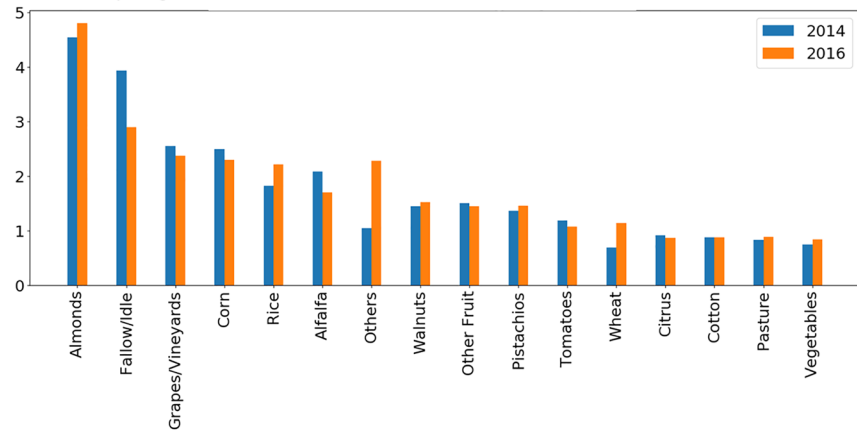
Compared to 2014, total crop consumptive water use increased by 9.6% in 2016 (Figure 10b), with an evapotranspiration rate of  $856 (\pm 306) \text{ mm yr}^{-1}$ , although the reference evapotranspiration from Spatial-CIMIS decreased by 4%. This increase in evapotranspiration was mostly caused by land-use changes with higher irrigated areas and crops with higher averaged water consumptive use (Figures 10a and 10c). Total irrigated agriculture land use increased by 7.0% in 2016, partly due to a 2,370  $\text{km}^2$  land-use conversion from fallow/idle lands in 2014 to cropland in 2016. A large portion of fallow land conversion grew rice (18%), wheat (16%), and perennial (9.7%) crops in 2016, leading to an increase of total water use by 1.3 tera-liters. Another major land-use change was the conversion from annual crops (386  $\text{km}^2$ ) to high water demand orchards, including almonds, walnuts, citrus, or grape in 2016, accounting for 1.5% of 2016 cropland and decreasing water use by 0.07 tera-liters due to the low evapotranspiration rate of young orchards.

### 3.5. Evapotranspiration Difference Among GSAs

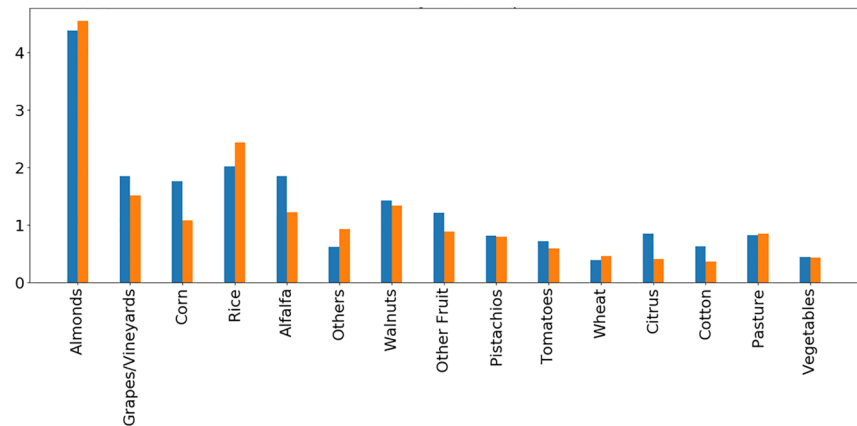
Across a total of 134 GSAs in the valley, the annual mean per-crop-area evapotranspiration rate was averaged at  $803 (\pm 154) \text{ mm yr}^{-1}$  in the 2014 water year, and it varied significantly among GSAs, with a CV of 19% and IQR of  $173 \text{ mm yr}^{-1}$  (Figure 11a). Most GSAs with a high ET rate ( $>1,000 \text{ mm yr}^{-1}$ ) were located in the north-eastern Central Valley, such as the Vina, Yuba Water Agency, and Southern Sutter Water District GSAs in Butte, Sutter, and Yuba counties. On the other hand, most GSAs with ET rates lower than



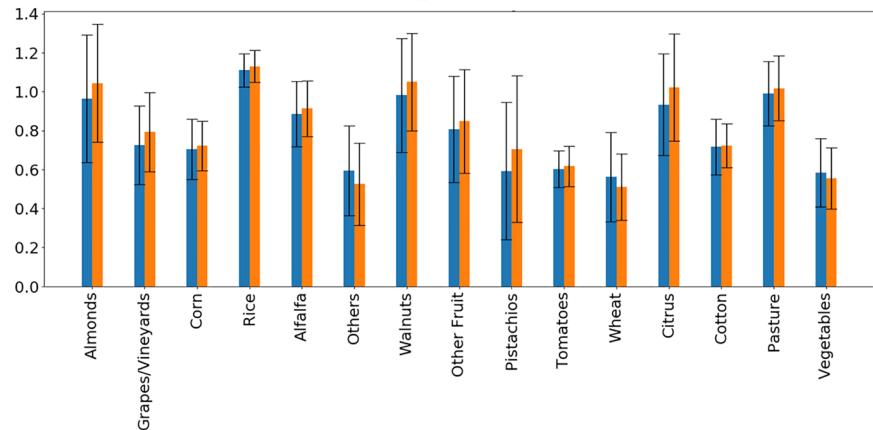
(a) Primary Agricultural Land use (Thousand km<sup>2</sup>)



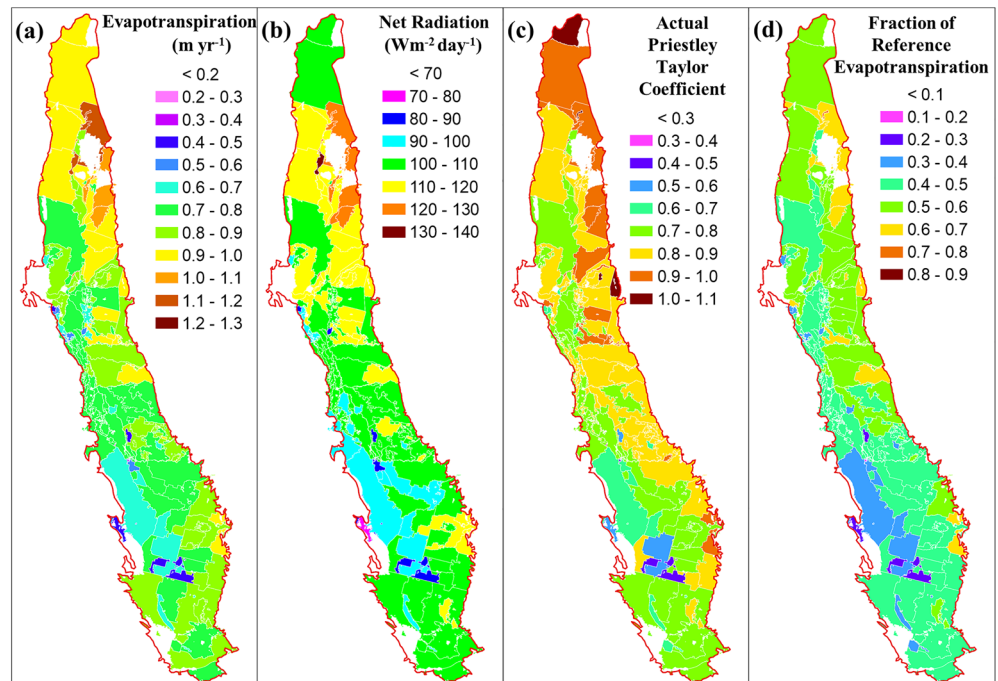
(b) Total Agricultural Consumptive Use (Tera-Liter yr<sup>-1</sup>)



(c) Per-area Agricultural Consumptive Use (m yr<sup>-1</sup>)



**Figure 10.** Primary agricultural land use (a) and agricultural consumptive water use (b, c) for each crop type in the Central Valley for 2014 and 2016 water years. Standard deviation of per-area evapotranspiration was also shown (error bars) in (c). Crops are sorted by the combined area in 2014 and 2016. Individual crops with an area <690 km<sup>2</sup> in either 2014 or 2016 were grouped into one of the following three categories, vegetables, other fruits, and others. Others include flowers, nursery, Christmas tree, miscellaneous deciduous, miscellaneous grain and hay, miscellaneous grasses, safflower, sunflowers, and young perennials.



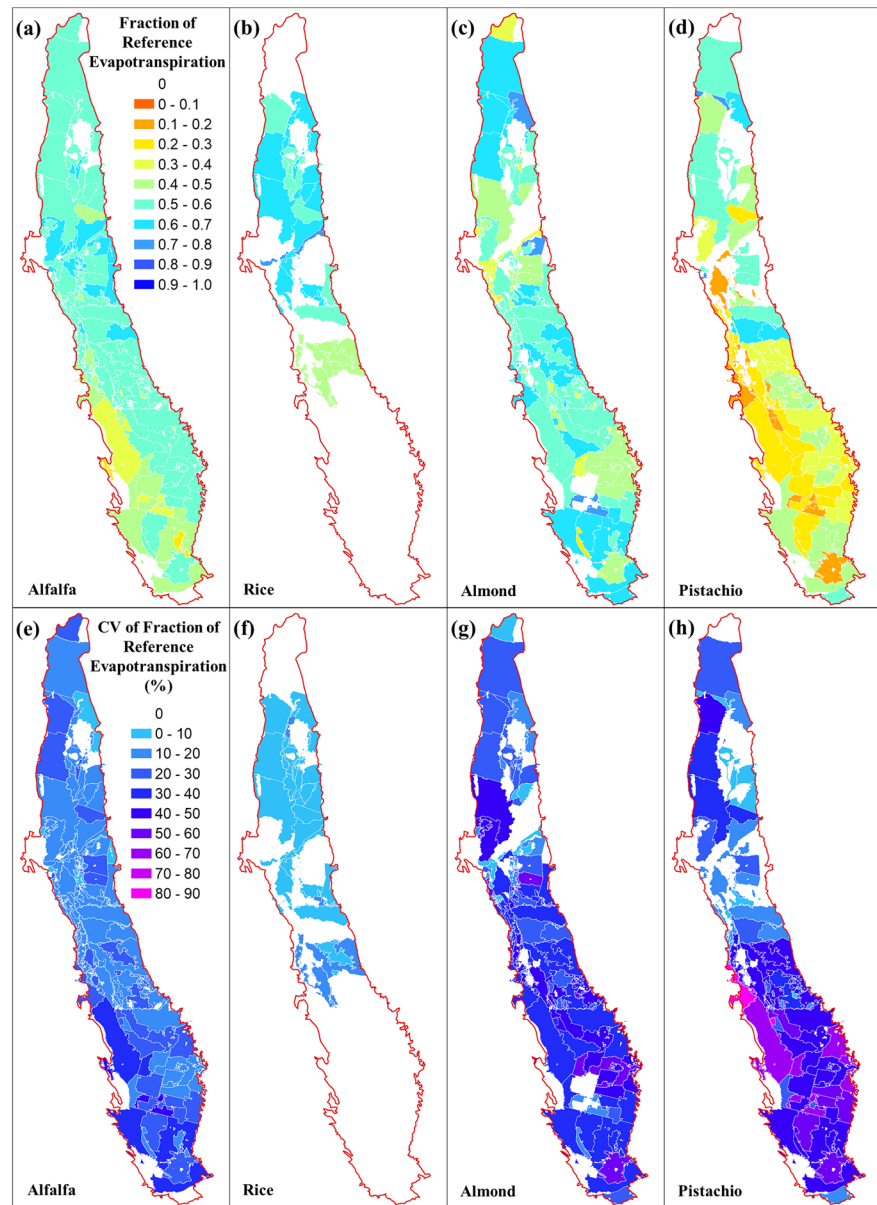
**Figure 11.** Spatial variation across Groundwater Sustainability Agencies in 2014 for (a) per-area evapotranspiration rate ( $\text{m yr}^{-1}$ ), (b) net radiation ( $\text{W m}^{-2} \text{ day}^{-1}$ ), (c) actual Priestley-Taylor coefficient, and (d) EToF over all cropland averaged by GSAs.

$700 \text{ mm yr}^{-1}$  were scattered across the south-western Central Valley, e.g., East Contra Costa Irrigation District GSA in the Contra Costa County, City of Tracy GSA, and the City of Stockton GSA in the San Joaquin County, El Rico GSA in the Kings county, and Pleasant Valley GSA and Westlands Water District GSA in the western part of Fresno county.

Variability of evapotranspiration rate among GSAs was primarily driven by nonmeteorological drivers. Across GSAs, we found that the evapotranspiration rate highly correlated with net radiation ( $r = 0.92$ ) and actual Priestley-Taylor coefficient ( $r = 0.88$ ) (Figures 11b and 11c). Many of these factors were regulated by land-use types, vegetation cover, and plant water stress status. The annual ETo ( $1,498 \pm 74 \text{ mm yr}^{-1}$ ) could only explain 4.5% of the variation in annual evapotranspiration rate among GSAs (Figure S9a). In contrast, EToF was the dominant driver of evapotranspiration rate variability among GSAs ( $r = 0.96$ ) (Figure 11d), mostly driven by crop types, e.g., rice with EToF of  $0.61 (\pm 0.06)$ , tomato  $0.33 (\pm 0.07)$ , almond  $0.52 (\pm 0.11)$ , and pistachio  $0.37 (\pm 0.16)$  summarized at the GSA scale.

Even for the same crop type, EToF varied significantly among GSAs for some tree crops and wheat  $0.36 (\pm 0.09)$ . The average almond EToF (Figure 12c), e.g., ranged from 0.25 in the City of Tracy GSA in Tracy county to 0.75 in Rock Creek Reclamation District GSA in Chico county. Pistachio's EToF was much lower in the majority of the western San Joaquin Valley areas (Figure 12d), probably due to the plant stress caused by salinity (Hanak et al., 2017; Jin et al., 2018; Letey, 2000). Citrus EToF ( $0.57 \pm 0.11$ ) had an IQR of 0.16 at the GSA scale. In contrast, the mean EToF showed much smaller variation among GSAs for the majority of annual crops such as alfalfa  $0.54 (\pm 0.08)$  (Figure 12a), rice  $0.61 (\pm 0.06)$  (Figure 12b), pasture  $0.57 (\pm 0.09)$ , and cotton  $0.35 (\pm 0.05)$ .

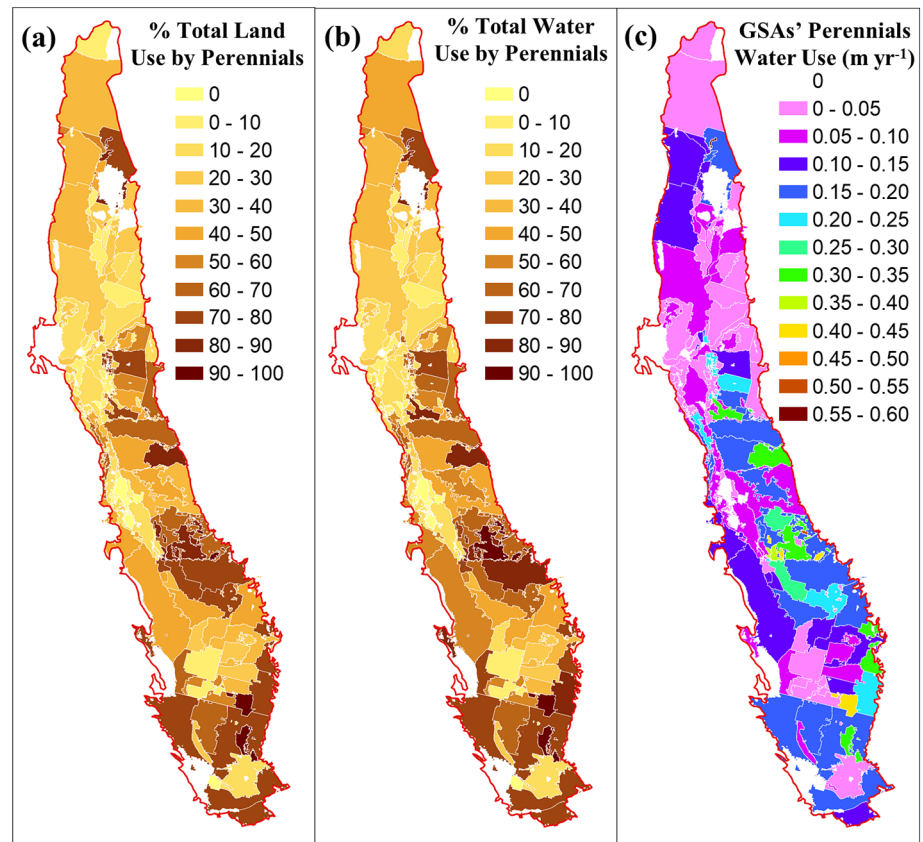
Within each GSAs, the annual EToF also showed large spatial variation, with a mean CV of 31% ( $\pm 12\%$ ) across all agricultural fields; Some GSAs with a lower evapotranspiration rate had the highest variability (Figures S9c and 11a), mostly located at and around the Westlands Water District region in the western-Fresno and Kings county. In addition to crop diversity within each GSA, significant variation of EToF was also found for each tree crop type, such as almonds and pistachios (Figures 12g and 12h), with IQRs of CVs among GSAs greater than 15%. For examples, the CVs of pistachio EToF within each GSAs had a mean



**Figure 12.** Mean (top) and CV (bottom) of the fraction of reference evapotranspiration by GSAs in 2014 for alfalfa (a, e), rice (b, f), almond (c, g), and pistachio (d, h).

of 34% ( $\pm 20\%$ ) and an IQR of 33% across GSAs, with the largest within-GSA variation found in the Central Delta-Mendota GSA; In the Southeast Kings GSA, CV of Pistachio EToF is 29%, much lower than its neighbor, Tri-County Water Authority GSA (64%). Other types with highly variable EToF (CV of 18+%  $\pm 10\%$ ) included almond, citrus, walnut, and wheat. In contrast, EToF was more homogeneous within GSA for alfalfa with a mean CV of 17% ( $\pm 7\%$ ) and IQR of 6% (Figure 12e), and rice (Figure 12f).

About 39 GSAs had >60% of agricultural land areas planted with perennial crops including almond, pistachio, citrus, walnut, and grape in 2014, which accounted for 76% of total agricultural water use by these GSAs and 27% of Central Valley's total agricultural water use in 2014 (Figure 13b). These GSAs will likely face greater vulnerability to prolonged drought due to the high cost of fallowing productive orchards. When dividing the total consumptive use of perennial crops by the GSA area (Figure 13c), we found that some small and medium-size GSAs, such as Delano-Earlimart Irrigation District GSA, Madera Water District



**Figure 13.** Percent of cropland (a) and of total water consumptive use (b) in 2014 by major perennial crops (almond, pistachio, citrus, walnut, and grape) in GSAs, and their total water consumptive use normalized by GSA area size (c).

GSA, and New Stone Water District GSA, will need to reserve a much greater depth ( $400 \text{ mm yr}^{-1}$ ) of groundwater storage to maintain the orchards during drought.

## 4. Discussion

### 4.1. Site-Level Performance

Our study showed that the semiempirical Priestley-Taylor algorithm, when calibrated with ground measurement data over diverse crop types and driven by Landsat Analysis Ready Data, improved the accuracy of the older 1 km MODIS-driven PT-0 model (Jin et al., 2011). The crop-specific Priestley-Taylor optimization performed consistently between the testing and independent data sets, and slightly better than the PT-JPL method (Fisher et al., 2008) (Figures 6 and S5). The generalized Priestley-Taylor optimization had a similar overall performance with PT-JPL when driven by the same input data. However, relatively larger uncertainties were found during nongrowing seasons, from November to March, when the evapotranspiration rate was relatively low. This was partly due to the limited field measurements data during winter and early spring for optimizing the sensitivity of actual Priestley-Taylor coefficients to the moisture content. Moreover, our Priestley-Taylor approach does not separate soil evaporation and plant transpiration. This introduces uncertainty in evapotranspiration estimates during nongrowing seasons when evapotranspiration is mainly driven by evaporation from the soil due to minimal canopy coverage or leaf area. For example, we did find that PT-JPL better captured the peak of the actual Priestley-Taylor coefficient for the corn site during the dormant season (Figure 5b), when PT-JPL's estimates showed that soil evaporation was the most significant component.

The uncertainty of our refined Priestley-Taylor approach here is similar to the DisALEXI model, as shown by the report from the Sacramento-San Joaquin Delta intercomparison project (Medellín-Azuara et al., 2018).

For additional reference, Anderson et al. (2018) reported that DisALEXI had an RMSE of 1.09 mm day<sup>-1</sup> at site number 1 (alfalfa) and 1.24 mm day<sup>-1</sup> at site number 24 (rice) when compared to daily measurements. Being a process-based model, DisALEXI does not depend on land-use maps and field measurements for calibration once validated. The semiempirical Priestley-Taylor approach, however, has the advantage of easy implementation, compared to other more sophisticated and computationally more expensive approaches.

#### 4.2. Regional Evapotranspiration Estimates

At a regional scale, the annual mean values of per-area water use of major crop types in the Central Valley (Table S7) estimated here are generally within the ranges reported in the literature (Burt et al., 2002; California Department of Water Resources, 2019a; Schauer & Senay, 2019). For example, DWR's water portfolio and balances data set, as part of DWR's 2018 Water Plan, reports that water requirement by corn ranges from 390 to 835 mm yr<sup>-1</sup> in 2014 across subregions (Detailed Analysis Units by County) of all planning areas in the Central Valley (California Department of Water Resources, 2019a, 2019d). Burt et al. (2002) estimated that corn in the Central Valley conventionally used 813 mm yr<sup>-1</sup> in a typical precipitation year. Our regional average of corn evapotranspiration (705 mm yr<sup>-1</sup>) was 16% more than DWR's average corn water requirement over planning areas (604 mm yr<sup>-1</sup>). Larger differences were found for alfalfa, pasture, wheat, almonds, pistachio, and vineyard, for which our regional averages were 30%–65% lower or higher than DWR's values. Over all 30-m pixels of agricultural lands in Central Valley (~25 thousand km<sup>2</sup>), the average annual evapotranspiration rate, estimated here, is higher than the estimates over the whole Central Valley (~47 thousand km<sup>2</sup>) by the BESS biophysical process-based model forced with 1 km satellite observations (Baldocchi et al., 2019). The discrepancy is likely due to the scale effect (Wu & Li, 2009) and differences in land cover maps. Larger pixels likely contain other land-use areas such as fallow, urban, water, and natural vegetation. Nonetheless, our estimates in 2014 align with the values reported in Schauer and Senay (2019) based on the SSEBop remote sensing evapotranspiration model driven by Landsat thermal data.

Our estimation of 19.6 tera-liter water consumption in 2014 was equivalent to 74% of DWR's estimate (26.2 tera-liter) over all planning areas within the Central Valley, which was derived from CalSIMETAW (Orang et al., 2013). Among the planning areas, the discrepancies ranged from -53.4% to -18.5%, with the most significant disagreement (<-50%) occurring in the southern and center-east of the San Joaquin Valley (planning areas 704, 708, 709 in Figure 1b). Similarly, previous studies in the Sacramento-San Joaquin Delta, a subset of the Central Valley, showed that remote sensing estimates are lower than CalSIMETAW's estimates by 6–24% (Medellín-Azuara et al., 2018; Paul et al., 2017). Over this Delta area, our crop-specific Priestley-Taylor method in this study estimated 1.20 tera-liter in 2016, very similar to the DisALEXI's estimate of 1.16 tera-liter in the water year 2016; both were about 80% of CalSIMETAW's estimates of 1.49 tera-liters, based on the published data summary table in Medellín-Azuara et al. (2018).

Two factors may have caused the discrepancy in regional estimates between PT-UCD and CalSIMETAW. First, CalSIMETAW's crop-coefficient approach implemented at a regional scale may overestimate actual evapotranspiration, because it did not account for the impacts of planting variabilities such as orchard age distribution and planting density, field conditions such as salinity and disease, and crop management like deficit irrigation. Second, the land-use map used by CalSIMETAW was different from the DWR's land-use map that we used here. For example, CalSIMETAW estimated 13.7, 23.9, and 23.9 km<sup>2</sup> of corn, alfalfa, and pasture in PA 704 in 2014, in contrast to our DWR's map-based estimates of 18.2, 21.4, and 9.3 km<sup>2</sup> of corn, alfalfa, and pasture.

#### 4.3. Implications for Water Resource Management

Currently, California's GSAs employ various approaches to estimate evapotranspiration in their water budget accounting and management plan development, causing systematic inconsistencies among GSAs. For example, the Olcese GSA near Bakersfield estimates monthly evapotranspiration from 1993 to 2015 using the METRIC method version by the Irrigation Training & Research Center (ITRC) at the California Polytechnic State University; North Kings GSA uses CA DWR's crop coefficients to estimate annual evapotranspiration rate over detailed analysis units from 1998 to 2010, while the Delano and Yuba GSAs use crop coefficients published by ITRC in 2003 and derived from an SEBAL-based evapotranspiration map in 2009,

respectively. Our study shows that the fractional of reference ET (EToF), or similarly crop coefficients, for most crops, varies spatially across and even within GSAs, and for some crops, EToF changes considerably between years. More consistent estimates with known uncertainty from a calibrated or thoroughly evaluated approach are needed to ensure consistent quantitative information for data-driven decisions for water planning. Our optimized Priestley-Taylor approach driven by remote sensing observations provides an efficient way to capture both spatial heterogeneity and temporal dynamics of water balance.

In particular, we found that orchards and wheat generally had a greater spatial variability of evapotranspiration and crop coefficients than other major crop types, across the Central Valley, within, and among GSAs. Age distribution and other stressors such as salinity likely contributed to such evapotranspiration variability for tree crops (Jin et al., 2018; UC-ANR, 2008, 2018). Among three major nut tree crops, pistachio had the lowest mean annual evapotranspiration rate ( $592 \pm 352$  mm yr<sup>-1</sup> in 2014), followed by walnut ( $981 \pm 291$  mm yr<sup>-1</sup> in 2014) and almond ( $964 \pm 328$  mm yr<sup>-1</sup> in 2014). Coincidentally, 26% of pistachio acreages in 2014, 18% of walnut in 2015, and 15% of almond in 2014 across California were nonbearing orchards (Administrative Committee for Pistachios, 2020; California Department of Food and Agriculture, 2020; US Department of Agriculture, 2020a; U.S. Department of Agriculture, 2020b). The high variability of wheat water use is likely due to cultivar and end-use for the crop (Fulton et al., 2006).

The rapid expansion of perennial crop acreage in the past two decades raises concerns about increasing and hardening water demand (Hanak et al., 2017; Johnson & Cody, 2015; Mall & Herman, 2019). As perennial crops have a sizeable initial investment cost, following perennial crops during drought results in greater economic losses than following annual crops. Therefore, GSAs with a high percentage of water use by perennials (Figure 13b) will likely experience challenges in implementing sustainability management during drought. To minimize economic loss during a severe multiyear drought, a large buffer between the sustainability threshold and actual water level should be maintained for those GSAs, that is, to prepare for a 5-year drought with conditions like 2014s, a groundwater buffer should be aimed with an approximate depth at least five times the values shown in Figure 13c, after accounting for surface water availability and total porosity of the aquifer.

The NASA ECOSTRESS mission (Fisher et al., 2020) has an ongoing partnership with USDA, states of California, Florida, and Iowa, and many water districts on using remote sensing evapotranspiration to better inform water resources management (Anderson et al., 2021). Anderson et al. (2021) also find that the improved temporal frequency of ECOSTRESS resulted in improved evapotranspiration estimates (RMSE improved by 65%) and captured peak growing season during which there were no Landsat acquisitions. The mission adopted both PT-JPL and DisALEXI to map evapotranspiration (L3 products), which serves as the basis for the derive L4 products, such as Water Use Efficiency (the ratio of gross primary productivity to actual evapotranspiration) and Evaporative Stress Index (the ratio of actual to reference evapotranspiration). ECOSTRESS also operationally provides the Priestley-Taylor potential evapotranspiration product, which has been demonstrated to be useful for water management agencies for spatial estimates of reference evapotranspiration (Kohli et al., 2020). Our model evaluation work suggests that PT-JPL's evapotranspiration estimates could potentially be further improved over irrigated croplands in agricultural regions with ample evapotranspiration measures over diverse crop types. On the other hand, our spatial estimates show that EToF, which is analogous to ECOSTRESS's Evaporative Stress Index, varies by crop types and within the Central Valley for the same crop types. Users of the Evaporative Stress Index product over Central Valley should also account for the threshold of water stress dependencies and variability by crop types and other factors such as orchard age and salinity.

#### 4.4. Model Limitations and Potential Improvement

Although overall our refined evapotranspiration estimation approach here has similar performance to that in more complex models such as DisALEXI (Anderson et al., 2018; Medellín-Azuara et al., 2018), there are still a few factors that can cause errors in our estimates. PT-UCD is a single-source approach. We noticed an overestimation of rice net radiation when the field was flooded, probably due to the challenges posed by heat storage in the water column and the effect of a wet surface, and an underestimation of net radiation over the two AmeriFlux corn sites between every April and July. We also found a larger uncertainty in estimating actual Priestley-Taylor coefficients for corn during the dormant season between January and April.

Although evapotranspiration during the nongrowing season accounts for a small fraction of total annual water use, explicit consideration of soil, and plant components of energy balance is expected to improve the accuracy of evapotranspiration estimates.

The errors of field measurements of evapotranspiration can propagate to the optimization. The energy balance closure issue, for example, has been well recognized for the eddy covariance measurements (Twine et al., 2000; Wilson et al., 2002). Baldocchi et al. (2016) and Eichelmann et al. (2018), for example, g., conducted several analyses at AmeriFlux sites in the Sacramento-San Joaquin Delta and found a closure of 79.3% in an alfalfa site, that is, the ratio of the sum of sensible and latent heat flux over the residual between net radiation and ground heat flux and storage, and 71% in a rice site. Their study suggests that incomplete storage calculation, rather than underestimation of eddy covariance measurements of fluxes, plays a major role in the lack of energy balance closure for their sites in the Sacramento-San Joaquin Delta. Therefore, we did not perform the correction for eddy covariance measurement sites from our data set.

Additional uncertainties can be introduced due to the varying footprint size of the flux towers and the scale mismatch between 30 m ET and tower measurements. We compared the annual evapotranspiration value extracted from a single Landsat pixel collocated with measurement sites and the mean (and standard deviation) of the values within the surrounding larger areas (Table S6). The differences in estimates between a  $90 \times 90$  m window and the single pixel were small, with the largest difference of  $-3.2\%$  occurred at site 18 in 2016. The differences generally increased with a larger footprint, depending on the heterogeneity of the areas, e.g., over a  $510 \times 510$  m window at site 16 (corn) in 2016 had the largest mean relative difference of  $-10.3\%$  from the corresponding center pixel value. Other studies also suggested that a rigorous footprint approximation is needed in future studies to make a fair comparison with field measurements (Anderson et al., 2018). For example, Kljun et al. (2015)'s flux footprint model could be implemented at flux tower sites to determine the weight and extent of the pixel window.

Compared to those driven by MODIS with daily revisiting (Jin et al., 2011), the evapotranspiration estimates derived from Landsat have the benefit of capturing finer spatial details, which is critical for water use assessment over a heterogeneous landscape. Landsat's 16-days repeating cycle, however, can potentially lead to uncertainty in water use monitoring, especially during the rainy season or during the rapid plant growth and senescence stages. In this study, the uncertainty due to the temporal interpolation of the missing days was found minimal overall, likely because the rainy season coincides with dormancy or the very beginning or ending of the crop growth for the majority of crops in Central Valley due to its Mediterranean climate (Figure S6, Tables 2 and S5). There were situations, for example, right after irrigation or right after harvesting for crops that undergo multiple harvests (alfalfa), when a relatively large error was introduced from the estimates interpolated from observations a few days apart. Future work is also needed to increase the temporal resolution of water use estimate by fusing Sentinel 2 A&B satellite observations every 5 days with Landsat data. A sophisticated data fusion technique will also improve the accuracy of evapotranspiration monitoring and assessment, by taking advantage of complementary observations from multiple sensors (Anderson et al., 2018).

The robustness of our optimization approach partly relies on the availability of multiple field measurements for diverse crop types across the Central Valley. The automatic workflow developed here allows for a continuous improvement of the optimization accuracy, by taking advantages of the increasingly available crop evapotranspiration measurements with the increased deployment of both research-grade and commercialized surface renewal stations in the state (Clay et al., 2019; Jin et al., 2018; Souto et al., 2019; Xue et al., 2020). Although the Priestley-Taylor parameters in this study were tailored for California's cropland, our data-model integration framework is generalizable to other regions. Once recalibrated and tested with local field data, the PT-UCD approach can be applied to monitor daily evapotranspiration and assess water use at various scales over regions besides the Central Valley.

## 5. Conclusion

To estimate agriculture consumptive water use at the field scale in Central Valley, we further refined the semiempirical Priestley-Taylor approach (Jin et al., 2011), by optimizing the actual Priestley-Taylor coefficient as a function of the leaf area index and moisture index with recently compiled ground measurements

of evapotranspiration for California's major crops. The net radiation estimates with Landsat Analysis Ready Data had an RMSE of  $25.8 \text{ W m}^{-2}$  and  $R^2$  of 0.74. Our study shows that the crop-specific optimization with field data is relatively robust, and the locally optimized approach captured well the regulation of plant growth and moisture stress on latent heat exchange and thus improved the accuracy of evapotranspiration estimation. The daily evapotranspiration, directly estimated during Landsat overpassing days under clear-sky and interpolated for other days, largely agreed well with the field measurements. The validation showed an  $R^2$  of 0.78 and an RMSE of  $0.95 \text{ mm day}^{-1}$ .

To facilitate the implementation of sustainable groundwater management plan in California, we applied this calibrated approach to the entire Central Valley, one of the world's most productive agricultural regions, to estimate evapotranspiration at 30-m resolution for water years 2014 and 2016 when high accuracy local land-use maps are available. The evapotranspiration rate averaged at  $820 \text{ mm yr}^{-1}$  and had a large spatial variability with a standard deviation of  $290 \text{ mm yr}^{-1}$  overall agricultural pixels in 2014. Total water uses in 2016 increased by 9.6%, as compared to 2014, mostly as a result of land-use conversion ( $2,370 \text{ km}^2$ ) from fallow/idle land in 2014 to cropland in 2016. When aggregated by the GSA boundaries, the annual evapotranspiration rate showed large variation among GSAs, i.e.,  $803 \pm 154 \text{ mm yr}^{-1}$  and a CV of 19% in 2014. This variability was mostly associated with variation in net radiation and the actual Priestley-Taylor coefficient or fraction of reference evapotranspiration, driven by crop type diversity and conditions. Perennial crops such as pistachios and almonds typically had much higher variability within and among GSAs than annual crops.

Our study demonstrates that remotely sensed evapotranspiration estimates can be combined with land-use maps to inform water resources planning and management. In particular, we provided more realistic estimates of crop coefficient and evapotranspiration for local water budget accounting, evaluation of crop water use variation within and among GSAs, and highlighted the importance of crop planning, orchard age structure, and other physiological stressors such as salinity on the trajectory of local orchard water use and demand.

#### Acknowledgments

The authors are grateful to all the field crew that collected field data, including J. Verfaillie and D. Szutu, and the California Department of Water Resources CIMIS program for providing spatial reference evapotranspiration data. The authors also thank Han Liu, Emily Hurry, Noah Bennett, and Abigail Neat for contributing to the workflow automation, and Dr. S. Liang and Dr. T. The author for sharing their coefficients for estimating albedo using Landsat 8 data. This project was partially funded by a consumptive use study for the Sacramento-San Joaquin Delta convened by the Office of the Delta Watermaster as part of the Sacramento-San Joaquin Delta Consumptive Water Use Project (Co-PIs J. Medellin-Azuara, Y. Jin, K. Paw U). Andy Wong is also supported by NASA JPL's ECOSTRESS project, AmericaView, and California's Space Grant. Y. Jin is also supported by the Agricultural Experiment Station project (CA-D-LAW-2296-H). J. B. Fisher, G. Rivera, C. M. Lee, and S. J. Hook carried out the research at the Jet Propulsion Laboratory, California Institute of Technology, under a contract with the National Aeronautics and Space Administration. California Institute of Technology. Government sponsorship acknowledged. Support was provided by the ECOSTRESS mission. Copyright 2019. All rights reserved.

#### Data Availability Statement

All data needed to reproduce the reported finding or conduct additional spatial analysis is made available on the HydroShare repository on April 10, 2021 (<http://www.hydroshare.org/resource/fe0ea8781ae44c97a-7c4a72be17dfd89>). The repository data set (3.12 GB) includes a single table containing model input data and daily averaged measurements from 26 sites (training, testing, and independent subsets of this table on Landsat overpassing days are also made available), calibrated parameters, additional evaluation (e.g., validation of the four subcomponents of net radiation, and time series for all sites), annual evapotranspiration maps (unit:  $\text{mm day}^{-1}$ , Gap-filled and nongap-filled), and summarized statistics for each GSA and DWR's planning area. Additional intermediate and output data and data visualization will be added to the repository upon request. All input data used by our model can be accessed from the websites as follows: Landsat Analysis Ready Data (<https://earthexplorer.usgs.gov/>); Spatial-CIMIS (<http://cimis.casil.ucdavis.edu/cimis/>); 2014 and 2016 Statewide Land-use Map (<https://data.cnra.ca.gov/dataset/statewide-crop-mapping>).

#### References

- Administrative Committee for Pistachios. (2020). *2019 pistachio bearing acreage, production and yield per acre*. Retrieved from <https://acpistachios.org/wp-content/uploads/2020/02/2019-Pistachio-Statistics-Revised-1.pdf>
- Akbar, R., Short Gianotti, D. J., Salvucci, G. D., & Entekhabi, D. (2019). Mapped hydroclimatology of evapotranspiration and drainage runoff using SMAP brightness temperature observations and precipitation information. *Water Resources Research*, *55*, 3391–3413. <https://doi.org/10.1029/2018WR024459>
- Allen, R. G., Burnett, B., Kramber, W., Huntington, J., Kjaersgaard, J., Kilic, A., et al. (2013). Automated calibration of the METRIC-Landsat evapotranspiration process. *Journal of the American Water Resources Association*, *49*(3), 563–576. <https://doi.org/10.1111/jawr.12056>
- Allen, R. G., Tasumi, M., & Trezza, R. (2007). Satellite-based energy balance for mapping evapotranspiration with internalized calibration (METRIC)-model. *Journal of Irrigation and Drainage Engineering*, *133*(4), 380–394. [https://doi.org/10.1061/\(ASCE\)0733-9437\(2007\)133:4\(380\)](https://doi.org/10.1061/(ASCE)0733-9437(2007)133:4(380))
- Anderson, M., Gao, F., Knipper, K., Hain, C., Dulaney, W., Baldocchi, D., et al. (2018). Field-scale assessment of land and water use change over the California delta using remote sensing. *Remote Sensing*, *10*(6), 889. <https://doi.org/10.3390/rs10060889>
- Anderson, M., Norman, J. M., Diak, G. R., Kustas, W. P., & Mecikalski, J. R. (1997). A two-source time-integrated model for estimating surface fluxes using thermal infrared remote sensing. *Remote Sensing of Environment*, *60*(2), 195–216. [https://doi.org/10.1016/S0034-4257\(96\)00215-5](https://doi.org/10.1016/S0034-4257(96)00215-5)



- Anderson, M. C., Allen, R. G., Morse, A., & Kustas, W. P. (2012). Use of Landsat thermal imagery in monitoring evapotranspiration and managing water resources. *Remote Sensing of Environment*, 122, 50–65. <https://doi.org/10.1016/j.rse.2011.08.025>
- Anderson, M. C., Norman, J. M., Mecikalski, J. R., Torn, R. D., Kustas, W. P., & Basara, J. B. (2004). A multiscale remote sensing model for disaggregating regional fluxes to micrometeorological scales. *Journal of Hydrometeorology*, 5(2), 343–363. [https://doi.org/10.1175/1525-7541\(2004\)005<0343:AMRSMF>2.0.CO;2](https://doi.org/10.1175/1525-7541(2004)005<0343:AMRSMF>2.0.CO;2)
- Anderson, M. C., Yang, Y., Xue, J., Knipper, K. R., Yang, Y., Gao, F., et al. (2021). Interoperability of ECOSTRESS and Landsat for mapping evapotranspiration time series at sub-field scales. *Remote Sensing of Environment*, 252, 112189. <https://doi.org/10.1016/j.rse.2020.112189>
- Baldocchi, D., Dralle, D., Jiang, C., & Ryu, Y. (2019). How much water is evaporated across California? A multiyear assessment using a biophysical model forced with satellite remote sensing data. *Water Resources Research*, 55, 2722–2741. <https://doi.org/10.1029/2018WR023884>
- Baldocchi, D., Falge, E., Gu, L., Olson, R., Hollinger, D., Running, S., et al. (2001). FLUXNET: A new tool to study the temporal and spatial variability of ecosystem-scale carbon dioxide, water vapor, and energy flux densities. *Bulletin of the American Meteorological Society*, 82(11), 2415–2434. [https://doi.org/10.1175/1520-0477\(2001\)082<2415:FANTTS>2.3.CO;2](https://doi.org/10.1175/1520-0477(2001)082<2415:FANTTS>2.3.CO;2)
- Baldocchi, D., Knox, S., Dronova, I., Verfaillie, J., Oikawa, P., Sturtevant, C., et al. (2016). The impact of expanding flooded land area on the annual evaporation of rice. *Agricultural and Forest Meteorology*, 223, 181–193. <https://doi.org/10.1016/j.agrformet.2016.04.001>
- Baldocchi, D. D., Hincks, B. B., & Meyers, T. P. (1988). Measuring biosphere-atmosphere exchanges of biologically related gases with micrometeorological methods. *Ecology*, 69(5), 1331–1340. <https://doi.org/10.2307/1941631>
- Bastiaanssen, W. G. M., Menenti, M., Feddes, R. A., & Holtslag, A. A. M. (1998). A remote sensing surface energy balance algorithm for land (SEBAL). 1. Formulation. *Journal of Hydrology*, 212–213, 198–212. [https://doi.org/10.1016/S0022-1694\(98\)00253-4](https://doi.org/10.1016/S0022-1694(98)00253-4)
- Burt, C. M., Mutziger, A., Howes, D., & Solomon, K. H. (2002). *Evaporation from irrigated agricultural land in California (Rep. No. 02-001)*. California Department of Food and Agriculture. (2018). *California agricultural production statistics*. Retrieved from <https://www.cdfa.ca.gov/statistics/>
- California Department of Food and Agriculture. (2020). *2019 California almond acreage report*. Retrieved from [https://www.nass.usda.gov/Statistics\\_by\\_State/California/Publications/Specialty\\_and\\_Other\\_Releases/Almond/Acreage/202004almac.pdf](https://www.nass.usda.gov/Statistics_by_State/California/Publications/Specialty_and_Other_Releases/Almond/Acreage/202004almac.pdf)
- California Department of Water Resources. (2005). *How much water has your crop used since your last irrigation?* Retrieved from [https://cimis.water.ca.gov/Content/pdf/Crop\\_Coefficients.pdf](https://cimis.water.ca.gov/Content/pdf/Crop_Coefficients.pdf)
- California Department of Water Resources. (2019a). *California water plan update 2018*. California Department of Water Resources.
- California Department of Water Resources. (2019b). *GSA map viewer*. Retrieved from <https://sgma.water.ca.gov/webgis/index.jsp?appid=gasmaster&rz=true>
- California Department of Water Resources. (2019c). *SGMA groundwater management*. Retrieved from <http://water.ca.gov/Programs/Groundwater-Management/SGMA-Groundwater-Management>
- California Department of Water Resources. (2019d). *Water plan water balance data*. Retrieved from <https://data.ca.gov/dataset/water-plan-water-balance-data>
- California Department of Water Resources. (2020a). *Handbook for water budget development with or without models* (pp. 446).
- California Department of Water Resources. (2020b). *Statewide crop mapping*. Retrieved from <https://data.cnra.ca.gov/dataset/statewide-crop-mapping>
- Castellvi, F., Snyder, R. L., Baldocchi, D. D., & Martínez-Cob, A. (2006). A comparison of new and existing equations for estimating sensible heat flux using surface renewal and similarity concepts. *Water Resources Research*, 42, W08406. <https://doi.org/10.1029/2005WR004642>
- Cawse-Nicholson, K., Fisher, J., & Wang, A. (2017). ECOSTRESS calibration and validation. Presented at the *ECOSTRESS Science Team Meeting*. Retrieved from [https://ecostress.jpl.nasa.gov/downloads/science\\_team\\_meetings/2017/day2/1\\_ECOSTRESS\\_calval.pdf](https://ecostress.jpl.nasa.gov/downloads/science_team_meetings/2017/day2/1_ECOSTRESS_calval.pdf)
- Clay, J., Paw U, K. T., McAuliffe, M., Schmiedeler, M., Mangan, M. R., & Lambert, J. J. (2019). Comparing in-situ measurements of evapotranspiration of crop and fallow fields in the Sacramento-San Joaquin River delta of California in 2018 using surface renewal and eddy covariance methods. In AGU Fall Meeting Abstracts (Vol. 41). Retrieved from <http://adsabs.harvard.edu/abs/2019AGUFM.B41L2473C>
- Consoli, S., O'Connell, N., & Snyder, R. (2006). Estimation of evapotranspiration of different-sized navel-orange tree orchards using energy balance. *Journal of Irrigation and Drainage Engineering*, 132(1), 2–8. [https://doi.org/10.1061/\(asce\)0733-9437\(2006\)132:1\(2\)](https://doi.org/10.1061/(asce)0733-9437(2006)132:1(2))
- Cook, M. J. (2014). *Atmospheric compensation for a Landsat land surface temperature product*. Rochester Institute of Technology. Retrieved from <https://scholarworks.rit.edu/cgi/viewcontent.cgi?article=9669&context=theses>
- Couvreur, V., Kandelous, M. M., Sanden, B. L., Lampinen, B. D., & Hopmans, J. W. (2016). Downscaling transpiration rate from field to tree scale. *Agricultural and Forest Meteorology*, 221, 71–77. <https://doi.org/10.1016/j.agrformet.2016.02.008>
- Cuenca, R., Ciotti, S., & Hagimoto, Y. (2013). Application of Landsat to evaluate effects of irrigation forbearance. *Remote Sensing*, 5(8), 3776–3802. <https://doi.org/10.3390/rs5083776>
- Cvijanovic, I., Santer, B. D., Bonfils, C., Lucas, D. D., Chiang, J. C. H., & Zimmerman, S. (2017). Future loss of Arctic sea-ice cover could drive a substantial decrease in California's rainfall. *Nature Communications*, 8(1), 1947. <https://doi.org/10.1038/s41467-017-01907-4>
- De Bruin, H. A. R. (1983). A model for the Priestley-Taylor parameter  $\alpha$ . *Journal of Climate and Applied Meteorology*, 22(4), 572–578. [https://doi.org/10.1175/1520-0450\(1983\)022<0572:amftpt>2.0.CO;2](https://doi.org/10.1175/1520-0450(1983)022<0572:amftpt>2.0.CO;2)
- D'Errico, J. (2020). *Slm-shape language modeling*. Retrieved from <https://www.mathworks.com/matlabcentral/fileexchange/24443-slm-shape-language-modeling>
- Duarte, H. F., Dias, N. L., & Maggioletto, S. R. (2006). Assessing daytime downward longwave radiation estimates for clear and cloudy skies in Southern Brazil. *Agricultural and Forest Meteorology*, 139(3), 171–181. <https://doi.org/10.1016/j.agrformet.2006.06.008>
- Dwyer, J. L., Roy, D. P., Sauer, B., Jenkerson, C. B., Zhang, H. K., & Lymburner, L. (2018). Analysis ready data: Enabling analysis of the Landsat archive. *Remote Sensing*, 10(9), 1363. <https://doi.org/10.3390/rs10091363>
- Eichelmann, E., Hemes, K. S., Knox, S. H., Oikawa, P. Y., Chamberlain, S. D., Sturtevant, C., et al. (2018). The effect of land cover type and structure on evapotranspiration from agricultural and wetland sites in the Sacramento-San Joaquin River Delta, California. *Agricultural and Forest Meteorology*, 256–257, 179–195. <https://doi.org/10.1016/j.agrformet.2018.03.007>
- Eichinger, W. E., Parlange, M. B., & Stricker, H. (1996). On the concept of equilibrium evaporation and the value of the Priestley-Taylor coefficient. *Water Resources Research*, 32(1), 161–164. <https://doi.org/10.1029/95WR02920>
- Escriva-Bou, A., Gray, B., Green, S., Harter, T., Jezdimirovic, J., Lund, J., et al. (2019). *Water and the future of the San Joaquin Valley*. <https://doi.org/10.13140/RG.2.2.24360.83208>
- Falk, M., Pyles, R. D., Ustin, S. L., Paw U, K. T., Xu, L., Whiting, M. L., et al. (2013). Evaluated crop evapotranspiration over a region of irrigated orchards with the improved ACASA-WRF model. *Journal of Hydrometeorology*, 15(2), 744–758. <https://doi.org/10.1175/JHM-D-12-0183.1>
- Faunt, C. C. (2009). *Groundwater availability of the Central Valley aquifer, California (No. Professional Paper 1766)*. U.S. Geological Survey. <https://doi.org/10.3133/fs20093057>

- Faunt, C. C., Sneed, M., Traum, J., & Brandt, J. T. (2016). Water availability and land subsidence in the Central Valley, California, USA. *Hydrogeology Journal*, 24(3), 675–684. <https://doi.org/10.1007/s10040-015-1339-x>
- Ferguson, L., Beede, R. H., Freeman, M. W., Haviland, D. R., Holtz, B. A., & Kallsen, C. E. (2005). *Pistachio production manual fruit and nut research and information center*. Davis, CA: University of California.
- Fisher, J. B. (2008). *Evapotranspiration Model (PT-JPL): MATLAB for spatial arrays*. Retrieved from <http://josh.yosh.org/>
- Fisher, J. B., Lee, B., Purdy, A. J., Halverson, G. H., Dohlen, M. B., Cawse-Nicholson, K., et al. (2020). ECOSTRESS: NASA's next generation mission to measure evapotranspiration from the international space station. *Water Resources Research*, 56, e2019WR026058. <https://doi.org/10.1029/2019WR026058>
- Fisher, J. B., Melton, F., Middleton, E., Hain, C., Anderson, M., Allen, R., et al. (2017). The future of evapotranspiration: Global requirements for ecosystem functioning, carbon and climate feedbacks, agricultural management, and water resources. *Water Resources Research*, 53, 2618–2626. <https://doi.org/10.1002/2016WR020175>
- Fisher, J. B., Tu, K. P., & Baldocchi, D. D. (2008). Global estimates of the land-atmosphere water flux based on monthly AVHRR and ISLSCP-II data, validated at 16 FLUXNET sites. *Remote Sensing of Environment*, 112(3), 901–919. <https://doi.org/10.1016/j.rse.2007.06.025>
- Fulton, A., Bali, K., Mousli, Z., & Jackson, L. (2006). *Small grains production manual, Part 5: Irrigation and water relations*. UC Davis. <https://doi.org/10.3733/ucanr.8168>
- Gao, B.-C. (1996). NDWI-A normalized difference water index for remote sensing of vegetation liquid water from space. *Remote Sensing of Environment*, 58(3), 257–266. [https://doi.org/10.1016/S0034-4257\(96\)00067-3](https://doi.org/10.1016/S0034-4257(96)00067-3)
- Garcia, L. E., Rodriguez, D. J., Wijnen, M. M. P., Pakulski, I., Serrat Capdevila, A., Garcia Ramirez, D. A., et al. (2016). *Earth observation for water resources management: Current use and future opportunities for the water sector (No. 104778)* (pp. 1–267). The World Bank. Retrieved from <http://documents.worldbank.org/curated/en/783571468196447976/Earth-observation-for-water-resources-management-current-use-and-future-opportunities-for-the-water-sector>
- Hanak, E. (2011). *Managing California's water: From conflict to reconciliation*. Public Policy Institute of CA.
- Hanak, E., Lund, J., Arnold, B., Escrivá-Bou, A., Gray, B., Green, S., et al. (2017). Water stress and a changing San Joaquin Valley. *Public Policy Institute of California*, 1, 5–48.
- Hart, Q. J., Brugnach, M., Temesgen, B., Rueda, C., Ustin, S. L., & Frame, K. (2009). Daily reference evapotranspiration for California using satellite imagery and weather station measurement interpolation. *Civil Engineering and Environmental Systems*, 26(1), 19–33. <https://doi.org/10.1080/10286600802003500>
- He, R., Jin, Y., Kandelous, M., Zaccaria, D., Sanden, B., Snyder, R., et al. (2017). Evapotranspiration estimate over an almond orchard using Landsat satellite observations. *Remote Sensing*, 9(5), 436. <https://doi.org/10.3390/rs9050436>
- Hemes, K. S., Chamberlain, S. D., Eichelmann, E., Anthony, T., Valach, A., Kasak, K., et al. (2019). Assessing the carbon and climate benefit of restoring degraded agricultural peat soils to managed wetlands. *Agricultural and Forest Meteorology*, 268, 202–214. <https://doi.org/10.1016/j.agrformet.2019.01.017>
- Hemes, K. S., Eichelmann, E., Chamberlain, S. D., Knox, S. H., Oikawa, P. Y., Sturtevant, C., et al. (2018). A unique combination of aerodynamic and surface properties contribute to surface cooling in restored wetlands of the Sacramento-San Joaquin Delta, California. *Journal of Geophysical Research: Biogeosciences*, 123, 2072–2090. <https://doi.org/10.1029/2018JG004494>
- Ji, L., Zhang, L., Wylie, B. K., & Rover, J. (2011). On the terminology of the spectral vegetation index (NIR – SWIR)/(NIR + SWIR). *International Journal of Remote Sensing*, 32(21), 6901–6909. <https://doi.org/10.1080/01431161.2010.510811>
- Jiang, C., & Ryu, Y. (2016). Multi-scale evaluation of global gross primary productivity and evapotranspiration products derived from Breathing Earth System Simulator (BESS). *Remote Sensing of Environment*, 186, 528–547. <https://doi.org/10.1016/j.rse.2016.08.030>
- Jin, Y., He, R., Marino, G., Whiting, M., Kent, E., Sanden, B. L., et al. (2018). Spatially variable evapotranspiration over salt affected pistachio orchards analyzed with satellite remote sensing estimates. *Agricultural and Forest Meteorology*, 262, 178–191. <https://doi.org/10.1016/j.agrformet.2018.07.004>
- Jin, Y., Randerson, J. T., & Goulden, M. L. (2011). Continental-scale net radiation and evapotranspiration estimated using MODIS satellite observations. *Remote Sensing of Environment*, 115(9), 2302–2319. <https://doi.org/10.1016/j.rse.2011.04.031>
- Johnson, R., & Cody, B. A. (2015). *California agricultural production and irrigated water use*. Sacramento, CA: Congressional Research Service Sacramento.
- Kljun, N., Calanca, P., Rotach, M. W., & Schmid, H. P. (2015). A simple two-dimensional parameterisation for Flux Footprint Prediction (FFP). *Geoscientific Model Development*, 8(11), 3695–3713. <https://doi.org/10.5194/gmd-8-3695-2015>
- Knipper, K. R., Kustas, W. P., Anderson, M. C., Alfieri, J. G., Prueger, J. H., Hain, C. R., et al. (2018). Evapotranspiration estimates derived using thermal-based satellite remote sensing and data fusion for irrigation management in California vineyards. *Irrigation Science*, 37, 431–449. <https://doi.org/10.1007/s00271-018-0591-y>
- Knox, S. H., Matthes, J. H., Sturtevant, C., Oikawa, P. Y., Verfaillie, J., & Baldocchi, D. (2016). Biophysical controls on interannual variability in ecosystem-scale CO<sub>2</sub> and CH<sub>4</sub> exchange in a California rice paddy. *Journal of Geophysical Research: Biogeosciences*, 121, 978–1001. <https://doi.org/10.1002/2015JG003247>
- Koeh, R., & Langat, P. (2018). Improving irrigation water use efficiency: A review of advances, challenges and opportunities in the Australian context. *Water*, 10(12), 1771. <https://doi.org/10.3390/w10121771>
- Kohli, G., Lee, C. M., Fisher, J. B., Halverson, G., Variano, E., Jin, Y., et al. (2020). ECOSTRESS and CIMIS: A comparison of potential and reference evapotranspiration in riverside county, California. *Remote Sensing*, 12(24), 4126. <https://doi.org/10.3390/rs12244126>
- Letey, J. (2000). Soil salinity poses challenges for sustainable agriculture and wildlife. *California Agriculture*, 54(2), 43–48. <https://doi.org/10.3733/ca.v054n02p43>
- Liang, S. (2001). Narrowband to broadband conversions of land surface albedo I. *Remote Sensing of Environment*, 76(2), 213–238. [https://doi.org/10.1016/S0034-4257\(00\)00205-4](https://doi.org/10.1016/S0034-4257(00)00205-4)
- Lynn, E. (2015). *California climate science and data for water resources management*. California Climate Science and Data.
- Macaulay, L., & Butsic, V. (2017). Ownership characteristics and crop selection in California cropland. *California Agriculture*, 71(4), 221–230. <https://doi.org/10.3733/ca.2017a0041>
- Mall, N. K., & Herman, J. D. (2019). Water shortage risks from perennial crop expansion in California's Central Valley. *Environmental Research Letters*, 14(10), 104014. <https://doi.org/10.1088/1748-9326/ab4035>
- MATLAB. (2018). *MATLAB and optimization toolbox release 2018a*. Natick, MA: The MathWorks, Inc.
- Medellín-Azuara, J., Paw U, K. T., Jin, Y., Jankowski, J., Bell, A. M., Kent, E., et al. (2018). *A comparative study for estimating crop evapotranspiration in the Sacramento-San Joaquin Delta*. Center for Watershed Sciences, University of California Davis. Retrieved from <https://watershed.ucdavis.edu/project/delta-et>

- Melton, F. S., Johnson, L. F., Lund, C. P., Pierce, L. L., Michaelis, A. R., Hiatt, S. H., et al. (2012). Satellite irrigation management support with the terrestrial observation and prediction system: A framework for integration of satellite and surface observations to support improvements in agricultural water resource management. *IEEE Journal of Selected Topics in Applied Earth Observations and Remote Sensing*, 5(6), 1709–1721. <https://doi.org/10.1109/JSTARS.2012.2214474>
- Nagler, P., Scott, R., Westenburg, C., Cleverly, J., Glenn, E., & Huete, A. (2005). Evapotranspiration on western U.S. rivers estimated using the enhanced vegetation index from MODIS and data from eddy covariance and Bowen ratio flux towers. *Remote Sensing of Environment*, 97(3), 337–351. <https://doi.org/10.1016/j.rse.2005.05.011>
- Norman, J. M., Anderson, M. C., Kustas, W. P., French, A. N., Mecikalski, J., Torn, R., et al. (2003). Remote sensing of surface energy fluxes at 101-m pixel resolutions. *Water Resources Research*, 39(8), 1221. <https://doi.org/10.1029/2002WR001775>
- Norman, J. M., Kustas, W. P., & Humes, K. S. (1995). Source approach for estimating soil and vegetation energy fluxes in observations of directional radiometric surface temperature. *Agricultural and Forest Meteorology*, 77(3), 263–293. [https://doi.org/10.1016/0168-1923\(95\)02265-Y](https://doi.org/10.1016/0168-1923(95)02265-Y)
- Oki, T., Valeo, C., & Heal, K. (2006). *Hydrology 2020: An integrating science to meet world water challenges*. IAHS-AISH Publication.
- Orang, M. N., Snyder, R. L., Shu, G., Hart, Q. J., Sarreshteh, S., Falk, M., et al. (2013). California simulation of evapotranspiration of applied water and agricultural energy use in California. *Journal of Integrative Agriculture*, 12(8), 1371–1388. [https://doi.org/10.1016/S2095-3119\(13\)60742-X](https://doi.org/10.1016/S2095-3119(13)60742-X)
- Paul, G., Schmid, B., Chong, C.-S., Roberson, M., Hawkins, T., Smith, A., et al. (2017). California actual evapotranspiration (CalEta) mapping program: A critical component for the development of water budget. Presented at the *Sustainability Groundwater Management Agency Conference*.
- Paw U, K. T., Baldocchi, D. D., Meyers, T. P., & Wilson, K. B. (2000). Correction of eddy-covariance measurements incorporating both advective effects and density fluxes. *Boundary-Layer Meteorology*, 97(3), 487–511. <https://doi.org/10.1023/A:1002786702909>
- Paw U, K. T., & Gao, W. (1988). Applications of solutions to non-linear energy budget equations. *Agricultural and Forest Meteorology*, 43(2), 121–145. [https://doi.org/10.1016/0168-1923\(88\)90087-1](https://doi.org/10.1016/0168-1923(88)90087-1)
- Paw U, K. T., Qiu, J., Su, H.-B., Watanabea, T., & Brunet, Y. (1995). Surface renewal analysis: A new method to obtain scalar fluxes. *Agricultural and Forest Meteorology*, 74(1), 119–137. [https://doi.org/10.1016/0168-1923\(94\)02182-J](https://doi.org/10.1016/0168-1923(94)02182-J)
- Priestley, C. H. B., & Taylor, R. J. (1972). On the assessment of surface heat flux and evaporation using large-scale parameters. *Monthly Weather Review*, 100(2), 81–92. [https://doi.org/10.1175/1520-0493\(1972\)100<0081:OTAOSH>2.3.CO;2](https://doi.org/10.1175/1520-0493(1972)100<0081:OTAOSH>2.3.CO;2)
- Ryu, Y., Baldocchi, D. D., Kobayashi, H., van Ingen, C., Li, J., Black, T. A., et al. (2011). Integration of MODIS land and atmosphere products with a coupled-process model to estimate gross primary productivity and evapotranspiration from 1 km to global scales. *Global Biogeochemical Cycles*, 25, GB4017. <https://doi.org/10.1029/2011GB004053>
- Schauer, M., & Senay, G. B. (2019). Characterizing crop water use dynamics in the central valley of California using Landsat-derived evapotranspiration. *Remote Sensing*, 11(15), 1782. <https://doi.org/10.3390/rs11151782>
- Shapland, T. M., Snyder, R. L., Smart, D. R., & Williams, L. E. (2012). Estimation of actual evapotranspiration in winegrape vineyards located on hillside terrain using surface renewal analysis. *Irrigation Science*, 30(6), 471–484. <https://doi.org/10.1007/s00271-012-0377-6>
- Smith, S. (2015). *Damage from sinking land costing California billions in infrastructure repairs*. NBC Bay Area. Retrieved from <https://www.nbcbayarea.com/news/local/damage-from-sinking-land-costing-california-billions-in-infrastructure-repairs/122810/>
- Snyder, R. L., & O'Connell, N. V. (2007). Crop coefficients for microsprinkler-irrigated, clean-cultivated, mature citrus in an arid climate. *Journal of Irrigation and Drainage Engineering*, 133(1), 43–52. [https://doi.org/10.1061/\(asce\)0733-9437\(2007\)133:1\(43\)](https://doi.org/10.1061/(asce)0733-9437(2007)133:1(43))
- Souto, C., Lagos, O., Holzapfel, E., Maskey, M. L., Wunderlich, L., Shapiro, K., et al. (2019). A modified surface energy balance to estimate crop transpiration and soil evaporation in micro-irrigated orchards. *Water*, 11(9), 1747. <https://doi.org/10.3390/w11091747>
- Storey, J., Lacasse, J., Smilek, R., Zeiler, T., Scaramuzza, P., Rengarajan, R., & Choate, M. (2005). *Image Impact of the Landsat 7 ETM+ Scan Line Corrector Failure*.
- Strom, S. (2014). *California's thirsting farmland*. The New York Times.
- Su, Z. (2002). The surface energy balance system (SEBS) for estimation of turbulent heat fluxes. *Hydrology and Earth System Sciences*, 6(1), 85–100. <https://doi.org/10.5194/hess-6-85-2002>
- Swinbank, W. C. (1951). The measurement of vertical transfer of heat and water vapor by eddies in the lower atmosphere. *Journal of Meteorology*, 8(3), 135–145. [https://doi.org/10.1175/1520-0469\(1951\)008<0135:TMOVTO>2.0.CO;2](https://doi.org/10.1175/1520-0469(1951)008<0135:TMOVTO>2.0.CO;2)
- Tucker, C. J. (1979). Red and photographic infrared linear combinations for monitoring vegetation. *Remote Sensing of Environment*, 8(2), 127–150. [https://doi.org/10.1016/0034-4257\(79\)90013-0](https://doi.org/10.1016/0034-4257(79)90013-0)
- Twine, T. E., Kustas, W. P., Norman, J. M., Cook, D. R., Houser, P. R., Meyers, T. P., et al. (2000). Correcting eddy-covariance flux underestimates over a grassland. *Agricultural and Forest Meteorology*, 103(3), 279–300. [https://doi.org/10.1016/S0168-1923\(00\)00123-4](https://doi.org/10.1016/S0168-1923(00)00123-4)
- UC-ANR. (2008). *Citrus ET by age—Kern County*. Retrieved from [http://ceker.ucanr.edu/Irrigation\\_Management/Citrus\\_ET\\_by\\_age/](http://ceker.ucanr.edu/Irrigation_Management/Citrus_ET_by_age/)
- UC-ANR. (2018). *Pistachio ET by age—Kern County*. Retrieved from [http://ceker.ucanr.edu/Irrigation\\_Management/Pistachio\\_ET\\_by\\_age/](http://ceker.ucanr.edu/Irrigation_Management/Pistachio_ET_by_age/)
- U.S. Department of Agriculture. (2020a). *2019 California Walnut Acreage Report*. Retrieved from [https://www.nass.usda.gov/Statistics\\_by\\_State/California/Publications/Specialty\\_and\\_Other\\_Releases/Walnut/Acreage/2020walac\\_revised.pdf](https://www.nass.usda.gov/Statistics_by_State/California/Publications/Specialty_and_Other_Releases/Walnut/Acreage/2020walac_revised.pdf)
- U.S. Department of Agriculture. (2020b). *Quick Stats: National Agricultural Statistics Service*. Retrieved from <https://quickstats.nass.usda.gov/>
- U.S. Department of Agriculture-National Agricultural Statistics Service. (2019). *2017 Census of agriculture—volume 1, chapter 2: County level data*. Retrieved from [https://www.nass.usda.gov/Publications/AgCensus/2017/Full\\_Report/Volume\\_1\\_Chapter\\_2\\_County\\_Level/California/](https://www.nass.usda.gov/Publications/AgCensus/2017/Full_Report/Volume_1_Chapter_2_County_Level/California/)
- U.S. Geological Survey. (2016). *Landsat 7 (Fact Sheet)*.
- Vinukollu, R. K., Wood, E. F., Ferguson, C. R., & Fisher, J. B. (2011). Global estimates of evapotranspiration for climate studies using multi-sensor remote sensing data: Evaluation of three process-based approaches. *Remote Sensing of Environment*, 115(3), 801–823. <https://doi.org/10.1016/j.rse.2010.11.006>
- Wilson, K., Goldstein, A., Falge, E., Aubinet, M., Baldocchi, D., Berbigier, P., et al. (2002). Energy balance closure at FLUXNET sites. *Agricultural and Forest Meteorology*, 113(1), 223–243. [https://doi.org/10.1016/S0168-1923\(02\)00109-0](https://doi.org/10.1016/S0168-1923(02)00109-0)
- Wu, H., & Li, Z.-L. (2009). Scale issues in remote sensing: A review on analysis, processing and modeling. *Sensors*, 9(3), 1768–1793. <https://doi.org/10.3390/s90301768>
- Xiao, M., Koppa, A., Mekonnen, Z., Pagán, B. R., Zhan, S., Cao, Q., et al. (2017). How much groundwater did California's Central Valley lose during the 2012–2016 drought? *Geophysical Research Letters*, 44, 4872–4879. <https://doi.org/10.1002/2017GL073333>

- Xue, J., Bali, K. M., Light, S., Hessels, T., & Kisekka, I. (2020). Evaluation of remote sensing-based evapotranspiration models against surface renewal in almonds, tomatoes and maize. *Agricultural Water Management*, 238, 106228. <https://doi.org/10.1016/j.agwat.2020.106228>
- Yao, Y., Liang, S., Li, X., Chen, J., Wang, K., Jia, K., et al. (2015). A satellite-based hybrid algorithm to determine the Priestley-Taylor parameter for global terrestrial latent heat flux estimation across multiple biomes. *Remote Sensing of Environment*, 165, 216–233. <https://doi.org/10.1016/j.rse.2015.05.013>

### **Reference From the Supporting Information**

- Allen, R. G., Morton, C., Kamble, B., Kilic, A., Huntington, J., Thau, D., et al. (2015). EEFlux: A Landsat-based evapotranspiration mapping tool on the Google earth engine. Paper presented at *2015 ASABE/IA irrigation symposium: Emerging technologies for sustainable irrigation-A tribute to the career of Terry Howell, Sr. conference proceedings* (pp. 1–11). American Society of Agricultural and Biological Engineers.